Anthropogenic CO_2 in the Atlantic Ocean

Nicolas Gruber[1]

Climate and Environmental Physics, Physics Institute, University of Bern, Bern, Switzerland

Abstract. The anthropogenic CO_2 in the Atlantic Ocean is separated from the large natural variability of dissolved inorganic carbon using the method developed by *Gruber et al.* [1996]. Surface concentrations of anthropogenic CO_2 are found to be highest in the tropical to subtropical regions and to decrease toward the high latitudes. They are very close to what is expected from thermodynamic considerations assuming that the surface ocean followed the atmospheric CO_2 perturbation. Highest specific inventories (inventory per square meter) of anthropogenic CO_2 occur in the subtropical convergence zones. Large differences exist between the North and South Atlantic high latitudes: In the North Atlantic, anthropogenic CO_2 has already invaded deeply into the interior; north of 50°N it has even reached the bottom. By contrast, waters south of 50°S contain relatively little anthropogenic CO_2, and hence specific inventories are very low. An anthropogenic CO_2 inventory of about 22 ± 5 Gt C is estimated for the Atlantic north of the equator for 1982, and 18 ± 4 Gt C is estimated for the Atlantic south of the equator for 1989. The Princeton ocean biogeochemistry model predicts anthropogenic CO_2 inventories of 20.0 Gt C (North Atlantic, 1982) and 17.7 Gt C (South Atlantic, 1989) for the same regions in good agreement with the observed inventories. Important differences exist on a more regional scale, associated with known deficiencies of the model.

1. Introduction

Oceanic uptake is a key part of the global budget of the CO_2 released to the atmosphere by human activities [*Houghton et al.*, 1996]. The methods for identifying the presence and quantifying the amount of anthropogenic CO_2 taken up by the oceans are manifold (see review by *Wallace* [1995]). Many of these proposed methods are based on observations not involving CO_2 directly [*Keeling and Shertz*, 1992; *Quay et al.*, 1992; *Tans et al.*, 1993; *Heimann and Maier-Reimer*, 1996]. While they are of prime importance for balancing the global anthropogenic carbon budget, they permit us to derive only global estimates of the uptake of anthropogenic CO_2 by the oceans. Information on regional distributions of the uptake is necessary, however, to validate ocean general circulation models, which constitute the only means by which future uptake of anthropogenic CO_2 can be assessed [*Sarmiento et al.*, 1995a; *Sarmiento and LeQuéré*, 1996; *Maier-Reimer et al.*, 1996]. The regional breakdown of the anthropogenic CO_2 uptake

also represents an important component in inverse atmospheric studies [*Enting et al.*, 1995].

One of the few concepts that yields direct anthropogenic CO_2 uptake estimates with regional information is the calculation of excess CO_2 as first independently proposed by *Brewer* [1978] and *Chen and Millero* [1979]. This method was applied in various regions of the world oceans [*Chen and Pytkowicz*, 1979; *Chen*, 1982; *Poisson and Chen*, 1987; *Chen*, 1993; *Chen et al.*, 1990; *Goyet and Brewer*, 1993; *Tsunogai et al.*, 1993; *Chen et al.*, 1995]. However, the Brewer and Chen/Millero approach is subject to rather large uncertainties and therefore has not found general acceptance [*Shiller*, 1981, 1982; *Broecker et al.*, 1985b]. *Gruber et al.* [1996] recently introduced an improved method to separate the anthropogenic CO_2 signal from the large natural variability of dissolved inorganic carbon in the oceans (see Figure 1). This method employs a quasi-conservative tracer ΔC^* that reflects the uptake of anthropogenic CO_2 and the air-sea disequilibrium when a water parcel loses contact with the atmosphere. This method was applied to data from the North Atlantic, and results were compared with those of two ocean circulation models of different complexity. Both the 2.5-dimensional ocean circulation model of *Stocker et al.* [1994] and the three-dimensional Princeton ocean biogeochemistry model (POBM) [*Sarmiento et al.*, 1995b] predicted anthropogenic CO_2 inventories in good agreement with the observations.

---

[1]Now at Program in Atmospheric and Oceanic Sciences, Princeton University, Princeton, New Jersey.
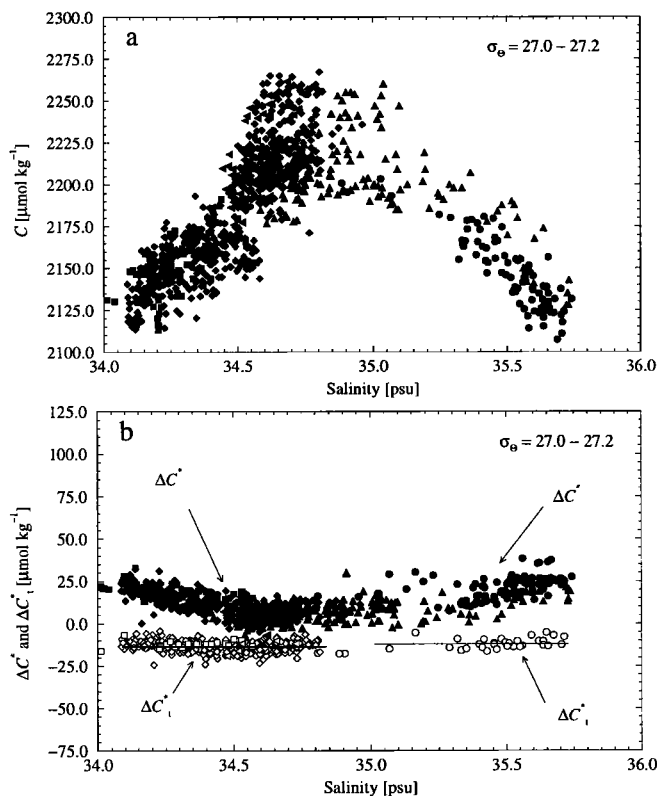
Figure 1. Illustration of the method to separate the anthropogenic CO$_2$ from the background variability of dissolved inorganic carbon (C) (modified from *Gruber et al.* [1996]). (a) Plot of C versus salinity in the σ_θ interval 27.0-27.2 in the Atlantic Ocean (Antarctic Intermediate Water). Diamonds denote samples from the South Atlantic Ventilation Experiment (SAVE) cruises, triangles denote samples from the Transient Tracer in the Oceans (TTO) Tropical Atlantic Study (TAS) cruises, circles denote samples from the TTO North Atlantic Study (NAS) cruises, leftward pointing triangles denote samples from the *Meteor* 15/3 cruise, and squares denote samples from the *Meteor* 11/5 cruise. Remineralization of C in the interior of the ocean causes the upward bow. (b) Plot of the quasi-conservative tracer ΔC^* versus salinity in the same σ_θ interval. After removal of the strong remineralization signal this tracer reflects only the uptake of anthropogenic CO$_2$ and the air-sea disequilibrium at the time the water parcel left the surface. The former causes the upward bow of ΔC^* toward the outcrops on the left and right side of the plot. The anthropogenic CO$_2$ signal can be removed by defining a modified tracer ΔC^*_t, for which information about the water age is needed. The amount of anthropogenic CO$_2$ can finally be determined by the difference between ΔC^* and ΔC^*_t.

The purpose of this paper is to extend this previous study to the entire Atlantic Ocean by including data from the South Atlantic Ventilation Experiment (SAVE) and two *Meteor* cruises (*Meteor* 11/5 and *Meteor* 15/3). This extension permits us to address explicitly the mixing between different end-members on

a specific potential density surface, a process that was neglected by *Gruber et al.* [1996].

The paper is organized as follows: In section 2 a summary of the separation technique for anthropogenic CO$_2$ is presented including a more detailed description of the treatment of end-member mixing. The data employed in this study are then briefly described. Afterward, the results are presented, discussed, and compared with results from the Princeton ocean biogeochemistry model.

2. Methods

I follow the technique developed by *Gruber et al.* [1996] to separate the anthropogenic CO$_2$ from the large background variability of dissolved inorganic carbon (C) in the oceans. The method is extended to treat explicitly the effect of mixing between the different end-members on a given potential density surface. The separation technique is based on the assumptions that (1) the natural carbon cycle has been operating in steadystate before the onset of the anthropogenic CO$_2$ perturbation, and (2) the carbon-to-oxygen and nitrate-to-oxygen stoichiometric ratios ($r_{C:O_2}$ and $r_{N:O_2}$) during photosynthesis, respiration, and remineralization are constant. This allows us to define a quasi-conservative tracer ΔC^*:

$$\Delta C^* = C - C_{eq}(S, T, \text{Alk}^0) \Big|_{f\text{CO}_2 = 280 \, \mu\text{atm}}$$
$$- r_{C:O_2} \left(O_2 - O_2^{\text{sat}} \right) \tag{1}$$
$$- \tfrac{1}{2} \left(\text{Alk} - \text{Alk}^0 + r_{N:O_2} \left(O_2 - O_2^{\text{sat}} \right) \right),$$

where C_{eq} is the equilibrium CO$_2$ concentration for a preindustrial atmospheric CO$_2$ fugacity of 280 μatm [*Neftel et al.*, 1994], S is the salinity, T is the temperature, Alk^0 is the preformed alkalinity, and O$_2$ and O$_2^{\text{sat}}$ are the in situ and saturation concentrations of oxygen, respectively. In order to maintain the conservative properties of ΔC^*, a linearized form of C_{eq} is used [*Gruber et al.*, 1996]. The preformed alkalinity Alk^0 is estimated from a multiple linear regression model using the conservative tracers salinity (S) and $PO = O_2 - r_{O_2:P}PO_4$ [*Broecker*, 1974] as independent variables [*Gruber et al.*, 1996]. The stoichiometric ratios determined by *Anderson and Sarmiento* [1994] are used throughout this study. These ratios $P:N:C_{org}:O_2$ = 1:16$\pm$1:117$\pm$14:$-$170$\pm$10 were found to be approximately independent of depth and ocean basin.

The variability of ΔC^* reflects only the ocean uptake of anthropogenic CO$_2$ (ΔC_{ant}) and the CO$_2$ disequilibrium at the time the water lost contact with the atmosphere plus any residual effects due to my choice of oxygen and alkalinity end-members and data uncertainties (ΔC_{diseq}). For any particular water parcel this total "effective" air-sea disequilibrium represents a mixture of the air-sea disequilibria of the n different end-members $\Delta C^i_{\text{diseq}}$:

$$\Delta C_{\text{diseq}} = \sum_{i=1}^{n} f^i \Delta C^i_{\text{diseq}}, \qquad (2)$$

where f^i denotes the relative contributions of the different end-members ($\sum f^i = 1$).

To determine the amount of anthropogenic CO$_2$, the additional assumptions are made that the water transport is predominantly along isopycnal surfaces and that the effective disequilibrium has stayed more or less constant within an outcrop region of a particular isopycnal surface interval. If these assumptions are correct, the concentration of ΔC^* on an isopycnal surface should reveal the history of the CO$_2$ uptake. *Gruber et al.* [1996] showed that this is, indeed, the case in the North Atlantic, supporting my a priori assumptions. I determine the total effective disequilibrium $\Delta C^i_{\text{diseq}}$ of the different end-members on a total of 32 isopycnal surface intervals in the Atlantic Ocean (see Table 1). The same isopycnal

Table 1. Mean Values of ΔC_{diseq} on Potential Density Surfaces in the Atlantic Ocean

Potential Density	$\Delta C^{\text{NA}}_{\text{diseq}}$, μmol kg^{-1}	σ, μmol kg^{-1}	N	$\Delta C^{\text{SA}}_{\text{diseq}}$, μmol kg^{-1}	σ, μmol kg^{-1}	N	$\Delta C^{\text{TA}}_{\text{diseq}}$, μmol kg^{-1}	σ, μmol kg^{-1}	N	Method[a]
				σ_θ *Surfaces*						
25.30	-19	5	5	4	7	15	13	1	2	2
25.60	-17	5	2	-5	5	22	17	2	3	2
25.90	-13	8	6	-12	6	23	9	4	4	2
26.20	-24	4	7	-17	2	9	4	4	14	2
26.50	-22	5	52	-15	5	25	-2	3	79	2
26.80	-12	3	34	-10	3	209	-5	3	25	2
27.10	-12	3	53	-13	3	303	-7	3	20	2
27.30	-14	4	20	-18	3	46				2
27.40	-17	4	13	-20	4	30				2
				σ_2 *Surfaces*						
36.45	-16	5	39	-17	3	34				2
36.55	-15	5	34	-20	2	26				2
36.65	-16	6	39	-19	5	15				2
36.75	-18	5	60	-20	3	9				2
36.85	-13	8	102	-17	7	47				1/2
36.95	-10	4	106	-17	5	48				1/2
37.00	-13	4	92	-14	4	108				1
37.05	-16	3	94	-16	3	110				1
				σ_4 *Surfaces*						
45.825	-16	3	51	-16	3	62				1
45.850	-16	4	49	-16	4	60				1
45.875	-15	4	68	-16	4	75				1
45.900	-16	3	39	-16	3	45				1
45.925	-15	3	28	-15	3	31				1
45.950	-15	3	15	-15	3	20				1
45.975				-14	3	27				1
46.000				-13	3	36				1
46.025				-12	3	30				1
46.050				-12	4	37				1
				σ_θ *Surfaces in the Greenland and Norwegian Seas*						
27.92	-36	5	8							2
27.96	-43	6	6							2
28.00	-41	5	6							2
28.04	-51	3	9							2
28.08	-56	2	34							2

Abbreviations are as follows: NA, North Atlantic end-member; SA, South Atlantic end-member; TA, Tropical Atlantic end-member; σ, standard deviation ; and N, number of observations.

[a]ΔC^* method is indicated as 1; ΔC^*_t method is indicated as 2.

surfaces as those of *Gruber et al.* [1996] are considered but augmented with four σ_4 surfaces representing the Antarctic Bottom Water in the South Atlantic. Observations above a depth of 100 m are excluded for the analysis, since this approach is limited to waters below the euphotic layer, which is on average about 50 to 100 m deep [*Morel*, 1988]. Furthermore, all stations located poleward of the wintertime outcrops as determined from the National Oceanic and Atmospheric Administration National Environmental Satellite Data and Information Service ocean atlas [*Levitus et al.*, 1994b; *Levitus and Boyer*, 1994] are removed. To obtain a continuous numerical representation of ΔC_{diseq} as a function of potential density, $\Delta C^i_{\text{diseq}}$ (σ), a smoothed spline function is used. The amount of anthropogenic CO_2 in the ocean ΔC_{ant} can finally be calculated by

$$\Delta C_{\text{ant}} = \Delta C^* - \sum_{i=1}^{n} f^i \Delta C^i_{\text{diseq}}(\sigma). \qquad (3)$$

The effective disequilibrium for the different end-members on an isopycnal surface σ, $\Delta C^i_{\text{diseq}}$ (σ), is determined using two different methods. The choice of method depends on the ventilation timescale of these isopycnal surfaces.

In the first method the variability of ΔC^* on deep ocean density surfaces far away from the outcrop is considered, where one can safely assume that there is no anthropogenic CO_2. ΔC^* in these "uncontaminated" regions then reflects just a mixture of the different end-member air-sea disequilibria $\Delta C^i_{\text{diseq}}$. In the deep Atlantic these end-members originate from the South or the North Atlantic high latitudes. The relative contribution (f_i) of these different end-member waters is determined using a two-end-member mixing model and the conservative tracer PO_4^* [*Broecker et al.*, 1991]. This tracer is defined as $PO_4^* = PO_4 - r_{P:O_2} O_2 - 1.95$. I chose $r_{P:O_2} = 1/(-170)$ [*Anderson and Sarmiento*, 1994] rather than the *Broecker et al.* [1991] original value of $1/(-175)$. The PO_4^* end-members for each investigated isopycnal interval are shown in Table 2. The effective air-sea disequilibrium for each end-member is then determined by averaging ΔC^* in the uncontaminated regions north and south of the equator:

$$\Delta C^i_{\text{diseq}} = \overline{\Delta C^*}\big|^{\text{reg}_i}_{\sigma=\text{const}}. \qquad (4)$$

This first method is used for all surfaces denser than $\sigma_2 = 36.95$ (average depth 2000 m) with the exception of the water masses in the Greenland and Norwegian Seas.

The ΔC^* method fails, however, for shallower and well-ventilated surfaces. Here anthropogenic CO_2 has already affected the entire density surface, and therefore no uncontaminated region can be found. For these density surfaces the ΔC_t^* method is employed. This method is based on the fact that the equilibrium con-

centration at the time this water parcel was last in contact with the atmosphere ($C_{\text{eq}}(t)$) can be estimated, once the age of that water parcel τ is known. Replacing C_{eq} in (1) by $C_{\text{eq}}(t)$ yields the modified tracer ΔC_t^*:

$$\begin{aligned} \Delta C_t^* &= C - C_{\text{eq}}(S, T, \text{Alk}^0, f CO_2(t_{\text{sample}} - \tau)) \\ &\quad - r_{C:O_2} \left(O_2 - O_2^{\text{sat}}\right) \qquad (5) \\ &\quad - \tfrac{1}{2} \left(\text{Alk} - \text{Alk}^0 + r_{N:O_2} \left(O_2 - O_2^{\text{sat}}\right)\right), \end{aligned}$$

where $f CO_2(t_{\text{sample}} - \tau)$ denotes the atmospheric CO_2 fugacity at the date when the water parcel was last in contact with the atmosphere. This date is calculated by subtracting the water age τ from the sampling date t_{sample}. The corresponding atmospheric CO_2 fugacity is estimated from a smoothed spline fit through atmospheric CO_2 data obtained from direct measurements after 1958 [*Keeling and Whorf*, 1994] and ice core data before 1958 [*Neftel et al.*, 1994]. This substitution removes the anthropogenic CO_2 signal from ΔC^* but does not correct for residual effects due to my choice of oxygen and alkalinity end-members. *Gruber et al.* [1996] argued that these residual effects should be relatively small. Hence ΔC_t^* reflects primarily the mixture of the different end-member air-sea disequilibria $\Delta C^i_{\text{diseq}}$. As for the deeper density surfaces, the conservative tracer PO_4^* is used to determine the contribution of the different end-members. On these shallow isopycnal surfaces I discriminate between end-members originating from the North Atlantic, the Mediterranean, the Tropical Atlantic, and the South Atlantic. However, for the Mediterranean water the same air-sea disequilibria as for the North Atlantic end-member are found. I therefore restrict myself to $n = 2$; that is, a two-end-member mixing model for all regions except the Greenland and Norwegian Seas is used. For surfaces less dense than $\sigma_\theta = 27.30$, mixing between a tropical end-member and a northern or southern end-member is assumed, depending on whether the station lies north or south of the equator. The exact source of the tropical end-member is not known, since the surfaces σ_θ 26.30–27.10 do not outcrop near the equator. The tropical end-member probably obtains its values through upwelling and/or cross-isopycnal mixing of deeper waters [*Kawase and Sarmiento*, 1985]. For the surfaces denser than $\sigma_\theta = 27.30$, mixing between the northern and southern end-members is assumed. Waters originating from the Mediterranean are treated as if they originate from the North Atlantic. In the Greenland and Norwegian Seas, only one end-member is considered. The chosen PO_4^* end-members for all investigated surfaces are listed in Table 2. The effective air-sea disequilibria for the different end-members are then determined by averaging the ΔC_t^* values in the regions where the end-member contribution is larger than 80% and the age is not older than 30 years thus

Table 2. End-Member Values of Conservative Tracer PO_4^* in the Atlantic Ocean

Potential Density	$PO_4^{*\ \mathrm{NA}}$, μmol kg^{-1}	$PO_4^{*\ \mathrm{ME}}$, μmol kg^{-1}	$PO_4^{*\ \mathrm{SA}}$, μmol kg^{-1}	$PO_4^{*\ \mathrm{TA}}$, μmol kg^{-1}
		σ_θ *Surfaces*		
25.30	-0.75		-0.50	-0.40
25.60	-0.75		-0.50	-0.20
25.90	-0.75		-0.40	-0.10
26.20	-0.70		-0.20	0.00
26.50	-0.50		-0.05	0.15
26.80	-0.20		0.50	0.20
27.10	0.10		1.50	0.80
27.30	0.50	0.15	1.70	
27.40	0.65	0.05	1.70	
		σ_2 *Surfaces*		
36.45	0.60	0.00	1.70	
36.55	0.70	0.10	1.65	
36.65	0.70	0.40	1.65	
36.75	0.80	0.40	1.60	
36.85	0.80	0.60	1.50	
36.95	0.76		1.48	
37.00	0.76		1.44	
37.05	0.76		1.42	
		σ_4 *Surfaces*		
45.825	0.76		1.40	
45.850	0.76		1.40	
45.875	0.76		1.50	
45.900	0.76		1.56	
45.925	0.76		1.56	
45.950	0.76		1.56	
45.975	0.76		1.56	
46.000	0.76		1.56	
46.025	0.76		1.56	
46.050	0.76		1.56	

Abbreviations are as follows: NA, North Atlantic end-member; ME, Mediterranean end-member; SA, South Atlantic end-member; and TA, Tropical Atlantic end-member.

$$\Delta C_{\mathrm{diseq}}^i = \overline{\Delta C_t^*}\big|_{\sigma=\mathrm{const}}^{\mathrm{reg}_i}. \qquad (6)$$

Two different techniques to estimate the water age τ are employed, depending on data availability. In the North Atlantic, concurrent tritium (^{3}H) and helium 3 (^{3}He) measurements are used to calculate the tritium-helium 3 age ($\tau_{\mathrm{T/He}}$) following the method of *Jenkins* [1987].

In the South Atlantic the anthropogenically produced chlorofluorocarbon CCl_3F (CFC 11) offers an alternative tracer dating technique [*Doney et al.*, 1997]. This CFC 11 based age ($\tau_{\mathrm{CFC\ 11}}$) is calculated using an atmospheric mixing ratio $X_{\mathrm{CFC\ 11}}$:

$$X_{\mathrm{CFC\ 11}} = \frac{[CCl_3F]}{K_{\mathrm{CFC\ 11}}(T,S)}, \qquad (7)$$

where $[CCl_3F]$ is the measured CFC 11 concentration and $K_{\mathrm{CFC\ 11}}(T,S)$ is the solubility of CFC 11 as a function of T and S according to *Warner and Weiss* [1985]. The calculated atmospheric mixing ratio $X_{\mathrm{CFC\ 11}}$ is then compared with past atmospheric mixing ratios of CFC 11 to determine a date of equilibration. For this purpose a reconstruction of the atmospheric CFC history is employed based on industrial release figures for the time before 1979 and on direct atmospheric measurements thereafter (S. Walker, P. Salameh, and R.F. Weiss, personal communication 1996).

This method of separating the anthropogenic CO_2 from the large variability of C is based on many assumptions (e.g., constant stoichiometric ratios and movement predominantly along isopycnal surfaces). However, the feasibility of these assumptions can be tested with the observational results. In general, it turns out that these

tests are consistent with my assumptions (see below and *Gruber et al.* [1996]). Nevertheless, there are three caveats that need further discussion. The first concerns the assumption that the air-sea disequilibrium has stayed constant over time. *Gruber et al.* [1996] estimated the signal in the air-sea disequilibrium which is caused by the anthropogenic transient to be about 5 μmol kg^{-1}. Such a trend should, in principle, be observed, but it is too small to be detected in the observations because of the uncertainties in the separation technique which are of the order of 9 μmol kg^{-1} [*Gruber et al.*, 1996].

The second caveat is related to my assumption of transport occurring predominantly along isopycnal surfaces thereby implicitly ignoring the effect of diapycnal mixing. In the thermocline of the open ocean, diapycnal diffusivities have been shown to be very small [e.g., *Ledwell et al.*, 1993], and scale analysis suggests that the contribution of diapycnal mixing is of minor importance. Even in places where diapycnal mixing becomes more important, I expect its influence on my estimate of anthropogenic CO_2 to stay rather small, because the linear part of the mixing process has already been taken into account. This is because the air-sea disequilibria are determined as a function of density and PO_4^*, which are either entirely (in the case of PO_4^*) or at least partially (in the case of density) conserved when mixed diapycnally. Additionally, the air-sea disequilibria are not varying strongly, so that even when the nonlinear effects become important, their effect on the estimated ΔC_{ant} should remain relatively small.

The third caveat concerns the assumption that the tritium-helium 3 ($\tau_{T/He}$) and CFC 11 ($\tau_{CFC\ 11}$) ages are equal to the true water ages. *Gruber et al.* [1996] discussed the case of the tritium-helium 3 age $\tau_{T/He}$ and argued that the difference between the true age and $\tau_{T/He}$ is relatively small for most regions of the ocean. This is because advection is thought to determine the transport in the interior of the ocean, and only if diffusion is dominant, can a significant deviation between the tritium-helium 3 age and the true water age occur [*Jenkins*, 1987; *Thiele and Sarmiento*, 1990]. More assumptions must be made in the case of the CFC 11 age $\tau_{CFC\ 11}$: The CFC 11 age is only equal to the true age if the water parcel was at equilibrium with the atmosphere at the time of entrainment and if the water parcel is transported along density surfaces without mixing ("piston flow"). *Doney et al.* [1997] investigated the differences between the tritium-helium 3 and the CFC 12 age along a meridional section in the eastern North Atlantic. They found a remarkably good agreement for water ages up to approximately 15 years with residuals only slightly greater than those expected from sampling error alone. Disparities between the two tracer ages increase sharply for ages approaching the elapsed

period since the bomb-tritium input in the early 1960s. *Doney et al.* [1997] explained these differences with the help of a simple two-dimensional gyre circulation model [*Musgrave*, 1990; *Thiele and Sarmiento*, 1990]. They showed that these disparities arise in regions of steep tracer gradients where the nonlinear effects become important. Nevertheless, the average difference between the true age and both tracer ages was found to be smaller than 2 years for waters younger than 15 years and up to 8 years for waters with an age of 30 years. An average uncertainty of 4 years relates to an uncertainty of about 3 μmol kg^{-1} in ΔC_t^*. This additional error is relatively small compared to the overall error in the determination of anthropogenic CO_2 of about 9 μmol kg^{-1} [*Gruber et al.*, 1996] (see section 3).

3. Data Considerations

Nutrient, C, Alk, and O_2 data from five different programs are used. These are the Transient Tracers in the Ocean North Atlantic Study (TTO NAS) program (1981) [*Physical and Chemical Oceanographic Data Facility*, 1986a; *Brewer et al.*, 1986], the Transient Tracers in the Ocean Tropical Atlantic Study (TTO TAS) program (1982–1983) [*Physical and Chemical Oceanographic Facility*, 1986b; *Brewer et al.*, 1986], the South Atlantic Ventilation Experiment (SAVE) program (1987–1989) [*Oceanographic Data Facility*, 1992a, b] (T. Takahashi, personal communication, 1995), the *Meteor* 11/5 cruise (World Ocean Circulation Experiment (WOCE) legs A12/A21, 1991) [*Chipman et al.*, 1994], and the *Meteor* 15/3 cruise (WOCE leg A9, 1991) [*Johnson et al.*, 1995]. The station locations of the cruises are shown in Figure 2. The revised version of the TTO NAS C data is used, recalculated from $f CO_2$ and Alk by *Takahashi and Brewer* [1986]. Alk has not been measured on *Meteor* 11/5 and has been measured only occasionally on *Meteor* 15/3. Alk was calculated for these cruises from C, pCO_2 measured at 20°C, T, S, phosphate, and silicate, employing a thermodynamic model of the inorganic carbon chemistry [*Fink*, 1996]. The dissociation constants in seawater of *Goyet and Poisson* [1989] for carbonic acid, of *Dickson* [1990] for boric acid, of *Millero* [1995] for water, of *Dickson and Riley* [1979] for phosphoric acid, and of *Millero* [1995] for silicic acid were used. The CO_2 solubility was computed from the formula given by *Weiss* [1974]. The total boron was estimated from a linear relationship with salinity given by *Uppström* [1974].

Where available, the standard hydrographic and carbon data were augmented with transient tracer data. Tritium and helium 3 measurements to calculate the tritium-helium 3 age are only available for TTO NAS. These data were obtained by the Woods Hole Oceanographic Institution Helium Isotope Laboratory (W.J.
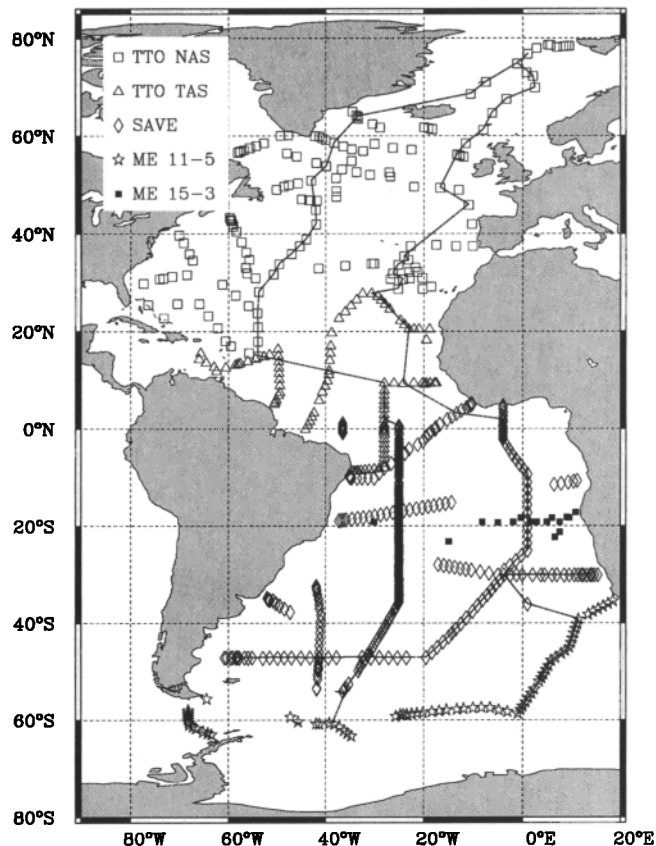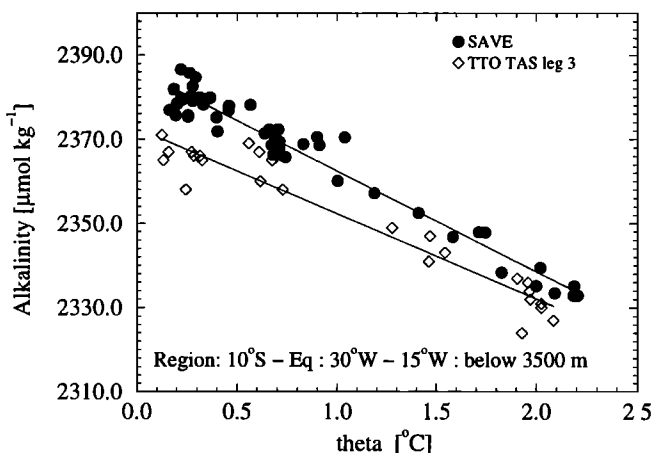
Figure 2. Hydrographic station locations of the TTO North Atlantic Study (TTO NAS, 1981)(open squares), TTO Tropical Atlantic Study (TTO TAS, 1982-1983) (triangles), the South Atlantic Ventilation Experiment (SAVE, 1987-1989)(diamonds), the *Meteor* 11/5 cruise (1991)(stars), and the *Meteor* 15/3 cruise (1991)(solid squares).

in the region from 10°S to the equator and from 30°W to 20°W has been found (see Figure 3). Other tracers do not indicate a significant change in water mass properties. I concluded that this difference is due to systematic measurement errors and therefore increased TTO TAS leg 3 alkalinities by 9 μmol kg^{-1}. All corrections are summarized in Table 3. Possible inaccuracies of the Atlantic carbon data were assessed by comparing them with the shore-based C and Alk measurements obtained by the Carbon Dioxide Research Group at the Scripps Institution of Oceanography (C.D. Keeling, personal communication, 1994). This comparison showed good agreement within the precision of the measurements [*Gruber et al.*, 1996].

The Atlantic data used in this study have been sampled over a period of 10 years. Temporal variability can cause problems in the separation technique because the assumption is made that the natural carbon cycle is operating in steady state. Decadal to interdecadal timescale variability in water mass properties has been reported for the northern North Atlantic [e.g., *Brewer et al.*, 1983; *Swift*, 1984; *Broecker*, 1985], for the subtropical North Atlantic [e.g., *Levitus et al.*, 1994a; *Parilla et al.*, 1994], and for the Argentine Basin in the South Atlantic [*Coles et al.*, 1996]. The influence of this variability on the marine carbon cycle is not known. *Gruber et al.* [1996] investigated the existence of large-scale changes in the water-mass and carbon-system characteristics by comparing reoccupied and closely revisited stations between the TTO NAS, TTO TAS, and SAVE cruises. They found no significant changes. This is not in contradiction to the reported findings of temporal

Jenkins, personal communication, 1995). Measurements of CCl₃F (CFC 11) to calculate the CFC 11 age are taken from the SAVE [*Weiss et al.*, 1993], *Meteor* 11/5 [*Chipman et al.*, 1994] and *Meteor* 15/3 [*Johnson et al.*, 1995] cruises.

When combining data from different cruises, it is necessary to insure the internal consistency of these data sets. *Gruber et al.* [1996] investigated the consistency of the C and Alk data from TTO NAS, TTO TAS, and SAVE by determining deep ocean (>3500 m) trends versus potential temperature in 10° latitude by 10° longitude areas which have been repeatedly sampled. They found systematic differences and corrected for them. The two *Meteor* cruises (ME 11/5 and ME 15/3) were checked by the same method, but no inconsistencies in the C and Alk data were found. However, significant deviations in the phosphate data of *Meteor* 11/5 exist and were corrected [*Gruber and Sarmiento*, 1997]. In addition, a previously overlooked systematic difference in Alk between TTO TAS leg 3 and SAVE of 9 μmol kg^{-1}

Figure 3. Alk versus potential temperature in the region from 10°S to 0° and from 30°W to 20°W and for depths below 3500 m in the equatorial Atlantic. Values for SAVE are shown by circles and for TTO TAS leg 3 are shown by diamonds. The lines represent the results of linear regressions. A mean difference of 9 μmol kg^{-1} is found between the two cruises.

Table 3. Summary of Corrections Applied to the C, Alk, and Phosphate Data in the Atlantic Ocean

Cruise	Leg	Stations	Correction[a]	Reference
TTO TAS	1	1-54	$Alk_{corr} = Alk_{meas} + 9$	[*Gruber et al.*, 1996]
TTO TAS	2	55-94	$C_{corr} = C_{meas} - 13$	[*Gruber et al.*, 1996]
TTO TAS	3	95-132	$Alk_{corr} = Alk_{meas} + 9$	this study
SAVE[b]	1	1-43	$C_{corr} = C_{meas} - 15$	[*Gruber et al.*, 1996]
SAVE[b]	1	1-43	$Alk_{corr} = Alk_{meas} - 19$	[*Gruber et al.*, 1996]
SAVE[b]	2	44-105	$C_{corr} = C_{meas} - 13$	[*Gruber et al.*, 1996]
SAVE[b]	2	44-105	$Alk_{corr} = Alk_{meas} - 12$	[*Gruber et al.*, 1996]
Meteor 11/5		102-179	$P_{corr} = P_{meas} - 0.5$	[*Gruber and Sarmiento*, 1997]

[a]Unit values given in μmol kg^{-1}.

[b]SAVE data have recently been recalculated (T. Takahashi, personal communication, 1997), and other correction factors might be necessary when a later data set is used.

variability because the investigated overlapping regions were far away from the regions where temporal variability has been reported. I repeated the analysis including the stations from *Meteor* 11/5 and *Meteor* 15/3 and came to the same conclusions. Therefore the possible temporal variability is neglected, and the data in the two ocean basins are combined as if they were synoptic. The time difference in sampling is, however, taken into account in the calculation of inventories (see section 4.4).

The evaluation of the amount of anthropogenic CO_2 in the oceans also requires estimates of the errors that arise from sampling and measurement and from uncertainties in the stoichiometric ratios and end-members. *Gruber et al.* [1996] discussed in detail the various contributions to the overall uncertainty of ΔC_{ant} by means of Gaussian error propagation. The overall uncertainty of ΔC_{ant} was estimated to about 9 μmol kg^{-1}. This error has been evaluated assuming a precision of 5 μmol kg^{-1} for the determination of C and for Alk. During the *Meteor* 11/5 and *Meteor* 15/3 cruises, modern coulometric methods have been used for C with a precision of about 1 μmol kg^{-1} [*Chipman et al.*, 1994; *Johnson et al.*, 1995]. This would lower the error for ΔC_{ant} considerably, but I suspect that the error over the entire basin is still of the order of 9 μmol kg^{-1}, since a good spatial coverage with these high-precision measurements is presently lacking.

To prepare plots of ΔC_{ant} on isopycnal surfaces, all observations within a specified potential density range and lying below 100 m are averaged. The randomly distributed data are first binned into a $2° \times 2°$ grid and then gridded using the objective mapping technique described by *LeTraon* [1990]. An autocorrelation function of Gaussian form is used, with a 1200-km radius of influence in the meridional as well as zonal direction.

4. Results and Discussion

4.1. ΔC^* and ΔC_t^*

Figure 4 shows ΔC^* as a function of latitude for two of the 12 deep isopycnal surfaces where ΔC_{diseq} has been determined by the ΔC^* method. These surfaces are the σ_2 interval 37.03–37.08, which represents the overflow waters of the Denmark Strait and the Iceland-Scotland ridge (depth range 3000–3200 m), and the σ_4 interval 45.913–45.938, which is the core of the Antarctic Bottom Water. ΔC^* increases on both surfaces toward the outcrops in the North and in the South Atlantic. This reflects the addition of anthropogenic CO_2. In the interior of these surfaces, ΔC^* is remarkably uniform within the uncertainty of ΔC^*. ΔC^* reflects here just the effective CO_2 air-sea disequilibrium at the time when a water parcel lost contact with the atmosphere, because one can safely assume that there is no anthropogenic CO_2. This near uniformity of ΔC^* supports my assumption that this air-sea disequilibrium stayed more or less constant over time. No difference between the regions from 20°S to the equator and from the equator to 20°N is discernible on either surface. The relative proportions of the southern and northern end-members in the region south of the equator are approximately 2:1 and are the inverse in the region north of the equator. This makes it difficult to determine the ΔC_{diseq} value of the pure end-member because any existing difference between the end-members would be reduced to a third. Nevertheless, in most cases considered, no or only a small difference could be identified between the two regions. Therefore the uncertainty for the ΔC_{diseq} values of the end-members should not be larger than the uncertainty given by the scatter of the data.

Figure 5 shows ΔC^* and ΔC_t^* versus CFC 11 age for four of the 15 density surfaces in the South Atlantic,
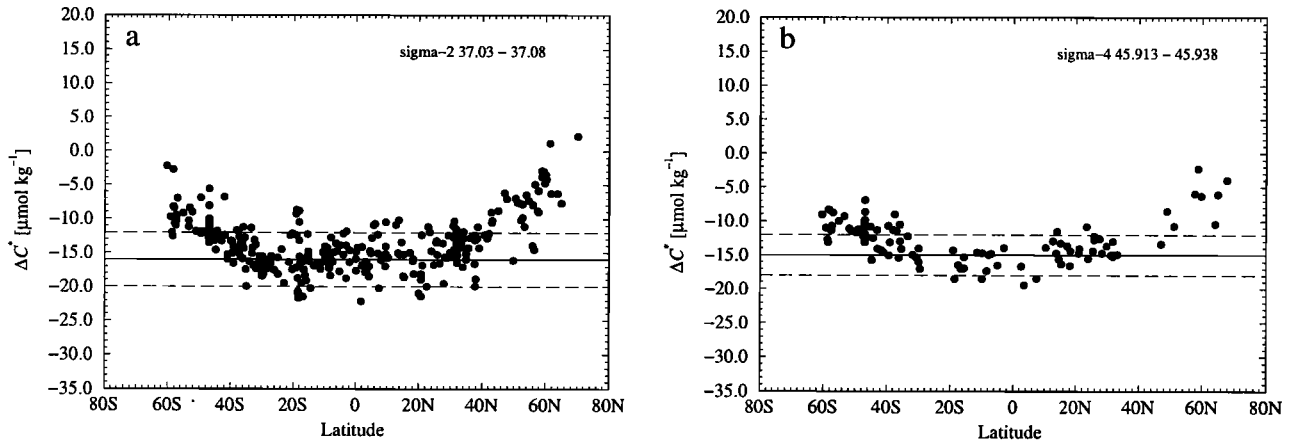
Figure 4. ΔC^* as a function of latitude along two deep isopycnal surface intervals in the Atlantic Ocean: (a) the σ_2 interval 37.03–37.08, which represents the Denmark Strait and Iceland-Scotland Overflow Waters, and (b) the σ_4 interval 45.913–45.938, which lies within the core of the Antarctic Bottom Water. The solid lines depict the average ΔC^* concentration in the regions from 20°S to the equator and from the equator to 20°N which have been used to determine ΔC_{diseq} for the southern and northern end-member, respectively. In both cases, no difference has been found between these two end-members. The dashed lines are drawn at ± 5 μmol kg^{-1} from the estimated ΔC_{diseq}. The upward trend near the outcrops in the south and the north is due to the uptake of anthropogenic CO₂.
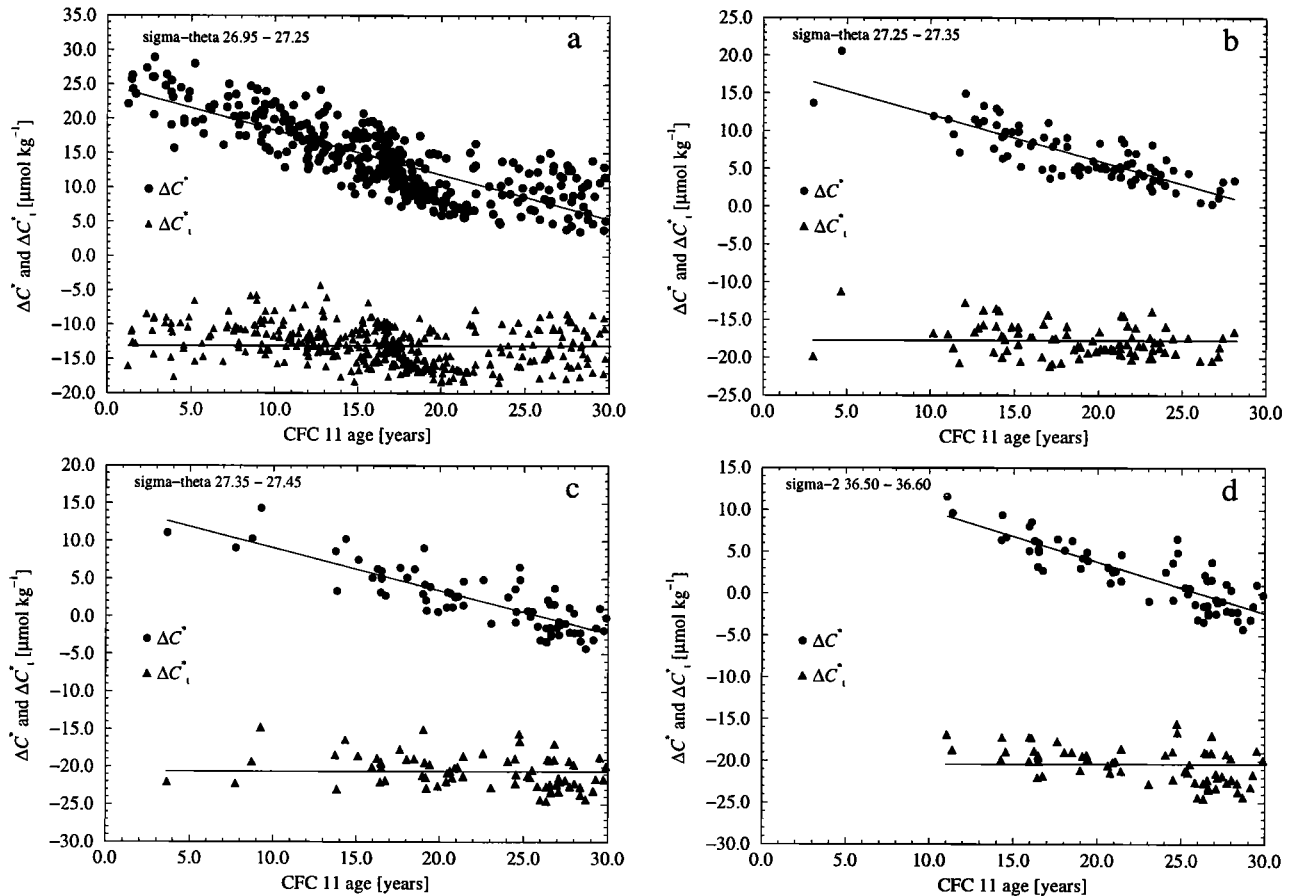
Figure 5. ΔC_t^* (triangles) and ΔC^* (circles) versus CFC 11 age along four isopycnal surface intervals in the South Atlantic. These surfaces include (a) the σ_θ interval 26.95-27.25 representing the Subpolar Mode Water, (b) the σ_θ interval 27.25-27.35 which lies within the upper Antarctic Intermediate Water, (c) the σ_θ interval 27.35-27.45 representing the Antarctic Intermediate Water, and (d) the σ_2 interval 36.50-36.60. The lines for ΔC^* are drawn to emphasize the trend and have been obtained by linear regression. The lines for ΔC_t^* represent the average.

where the ΔC_t^* method has been used to determine the air-sea disequilibrium of CO_2. The reader is referred to Gruber et al. [1996] for a discussion of the distribution of ΔC_t^* in the North Atlantic. The surfaces shown are the σ_θ interval 26.95–27.25 (depth range 400–700 m) which represents the Subantarctic Mode Water [Sievers and Nowlin, 1984], the σ_θ interval 27.25–27.35, the σ_θ interval 27.35–27.45 (depth range 800–1200 m) lying within the tongue of the Antarctic Intermediate Water, and the σ_2 interval 36.50–36.60 (depth range 1000–1300 m) representing the upper branch of the Circumpolar Deep Water (CDW) [Reid et al., 1977]. No such plots can be shown for the more shallow surfaces in the South Atlantic, since the distribution of ΔC^* and ΔC_t^* on these surfaces is strongly determined by the mixing between the tropical and the southern end-members. The surfaces shown in Figure 5 have no tropical end-member, and the contribution of the northern end-members is very small for waters less than 30 years old. Figures 5a - 5d can therefore be discussed as if all waters originate from the South Atlantic only.

On all surfaces, ΔC^* decreases with increasing water age. This decrease reflects the invasion of anthropogenic CO_2, since atmospheric $f CO_2$ was lower when the older water was last in contact with the atmosphere. After removing this effect from ΔC^* by replacing C_{eq} with $C_{eq}(t)$, the resulting ΔC_t^* shows more or less constant values within the uncertainties of the scatter. ΔC_t^* reflects the effective air-sea disequilibrium when the water parcel left contact with the atmosphere. Therefore this near constancy of ΔC_t^* confirms my a priori assumption that the effective air-sea disequilibrium in the outcrop region of a specific density surface remained constant over time. Gruber et al. [1996] have shown that this is also the case in the North Atlantic. The effective air-sea disequilibrium ΔC_{diseq} is determined finally by averaging all ΔC_t^* values within a isopycnal interval using only values with water ages younger than 30 years.

4.2. Air-Sea Disequilibrium

A summary of the effective air-sea disequilibria for the different end-members, ΔC_{diseq}^i, found on the investigated density surface intervals, is given in Table 1 and depicted in Figure 6. Also shown are the smoothed spline curves, which are used for the final estimate of ΔC_{ant}. All surfaces deeper than σ_θ 26.40 (average depth 200–300 m) have negative ΔC_{diseq}. This is because these surfaces outcrop in temperate to high-latitude regions characterized by wintertime cooling, which causes the CO_2 fugacity to drop below the atmospheric equilibrium fugacity. The North Atlantic end-member ΔC_{diseq} does not vary greatly over the entire water column with values between -24 μmol kg^{-1} and -10 μmol kg^{-1} as discussed by Gruber et al. [1996].

The ΔC_{diseq} end-member values of the tropical Atlantic deviate strongly from the pattern of the North Atlantic end-members. Positive values of ΔC_{diseq} are found for all σ_θ surfaces <26.20, with a maximum of 17 μmol kg^{-1}. Since these surfaces do not outcrop in the tropical region, processes in the interior must be responsible for setting these high end-member values. I do not clearly understand these processes, but it is possible that upwelling and/or cross isopycnal mixing of waters rich in C caused by the remineralization of organic matter create these high end-member ΔC_{diseq}. During this
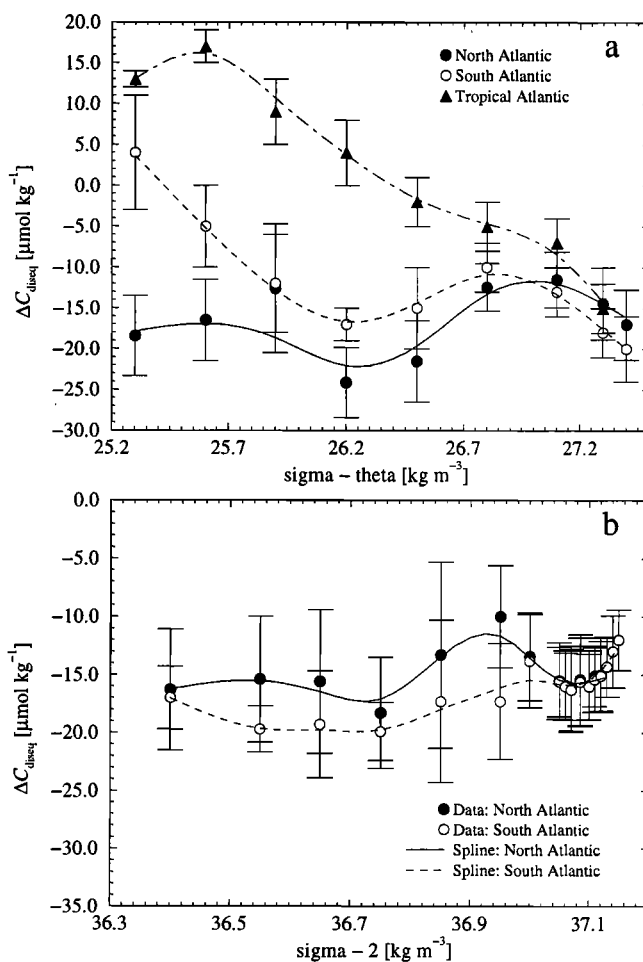
Figure 6. Plot of the estimated ΔC_{diseq}^i versus potential density for the different density intervals. (a) End-member air-sea disequilibria for the North Atlantic (solid circles), South Atlantic (open circles) and tropical Atlantic (triangles) are shown for the σ_θ surfaces 25.30–27.40. The smoothing spline fits have been computed with a stiffness parameter of 0.9998. (b) End-member air-sea disequilibria for the North Atlantic (solid circles) and South Atlantic (open circles) depicted for the σ_2 surfaces from 36.45–37.05 and the σ_4 surfaces 45.825–46.050 (converted to the appropriate σ_2 value). The smoothing spline fits have been calculated with a stiffness parameter of 0.999997.

process, oxygen must be at least partially replenished from the atmosphere, whereas C is not, which is feasible since oxygen has about a 10 times lower characteristic air-sea gas exchange time than CO_2 [*Broecker and Peng*, 1974]. The influence of these processes decreases with increasing potential density until no distinct tropical end-member is discernible at σ_θ 27.30.

The ΔC_{diseq} values of the South Atlantic end-members lie between the tropical and North Atlantic end-members in the upper ocean. A positive value is found for the most shallow surface investigated ($\sigma_\theta = 25.30$). The σ_θ surfaces 26.05–26.65 show a similar minimum as observed in the North Atlantic. Below σ_θ 26.80, differences between the southern and northern end-members are small and mostly within the uncertainty in the determination of ΔC_{diseq}. Exceptions are the σ_2 surfaces between 36.90 and 37.03. These density surfaces represent the North Atlantic Deep Water (NADW) in the north and the Circumpolar Deep Water (CDW) in the south [*Reid et al.*, 1977].
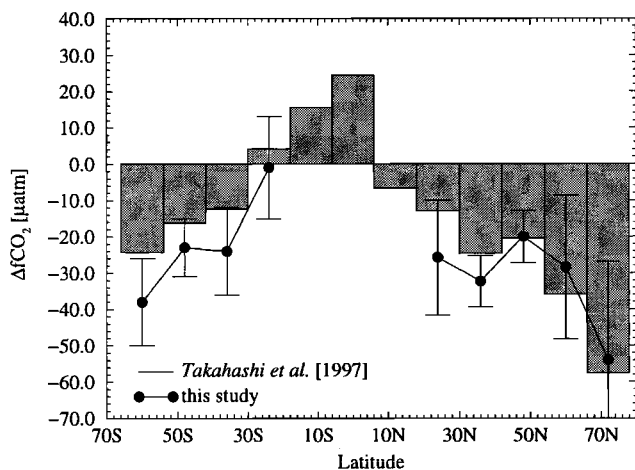
How consistent is this pattern of CO_2 air-sea disequilibrium reconstructed from data of the interior of the ocean with direct observations of $\Delta f CO_2$ at the sea surface? I calculated zonal mean $\Delta f CO_2$ from ΔC_{diseq} following the methods described by *Gruber et al.* [1996] and compared them with wintertime observations of $\Delta f CO_2$ in the northern and southern hemispheres (December-February and June-August, respectively) as recently compiled by *Takahashi et al.* [1997] (Figure 7). In this analysis, data from isopycnal surfaces which outcrop in the seasonal sea-ice zone have not been included. As already discussed by *Gruber*

Figure 7. Comparison of the Atlantic Ocean zonal mean air-sea difference of fCO_2 and ΔfCO_2, between the observational estimates of *Takahashi et al.* [1997] and the estimates based on ΔC_{diseq}. The observations are averages for the winter months in the northern and southern hemispheres (December to February and June to August, respectively).

et al. [1996], the North Atlantic shows very good agreement between the $\Delta f CO_2$ estimated from data of the interior of the ocean and the direct observations. In the South Atlantic, my $\Delta f CO_2$ are on average about 10 μatm lower than the estimates of *Takahashi et al.* [1997]. Given the large uncertainties in determining $\Delta f CO_2$ from ΔC_{diseq}, this difference is barely significant. It is also possible that *Takahashi et al.* [1997] may have underestimated the wintertime $\Delta f CO_2$ since they had only very limited wintertime data available in the South Atlantic. In summary, this independent test of my approach to determine the air-sea disequilibrium increases the confidence in the determination of ΔC_{diseq} and hence also ΔC_{ant}.

4.3. Distribution of Anthropogenic CO₂ in the Atlantic Ocean

Horizontally averaged profiles of anthropogenic CO_2 in 10° latitude belts from 70°S to 80°N were calculated by averaging all data within a given depth bin and latitude belt (see Figure 8). Negative values of the estimated ΔC_{ant} are kept as negative values in the averaging process. In the North Atlantic northward of 10°N the profiles are nearly identical to those shown by *Gruber et al.* [1996, Figure 8] despite the inclusion of end-member mixing in the determination of ΔC_{ant}. This confirms the previous assumption of *Gruber et al.* [1996] that the influence of the tropical and southern end-members is small and can be neglected in the North Atlantic north of 15°N.

The near-surface concentrations of ΔC_{ant} are highest in the tropical to subtropical regions (40–60 μmol kg^{-1}) and decrease toward the high latitudes (20–30 μmol kg^{-1}). This is in good agreement with expectations based on thermodynamic considerations (Revelle factor) and the assumption that the surface ocean closely followed the anthropogenic CO_2 increase in the atmosphere [*Gruber et al.*, 1996]. In the tropical regions (20°S to 20°N), ΔC_{ant} rapidly decreases with depth to about 15 μmol kg^{-1} at 1000 m and to below 5 μmol kg^{-1} at about 1800 m. This shallow penetration is due to the shallow but strong pycnocline and the poor lateral ventilation [*Doney and Bullister*, 1992]. In the subtropical latitude belts of both southern and northern hemispheres (40°S to 20°S and 20°N to 40°N, respectively) the concentration of ΔC_{ant} in the main thermocline is higher, and ΔC_{ant} penetrates deeper. These regions are characterized by Ekman convergence where ΔC_{ant} is expected to accumulate [*Broecker et al.*, 1985a; *Sarmiento et al.*, 1992]. The symmetry between the two hemispheres breaks down farther toward the poles. While the latitude belts between 40° and 50° show a similar vertical pattern, the high-latitude profiles in the North and South Atlantic are very different. In the
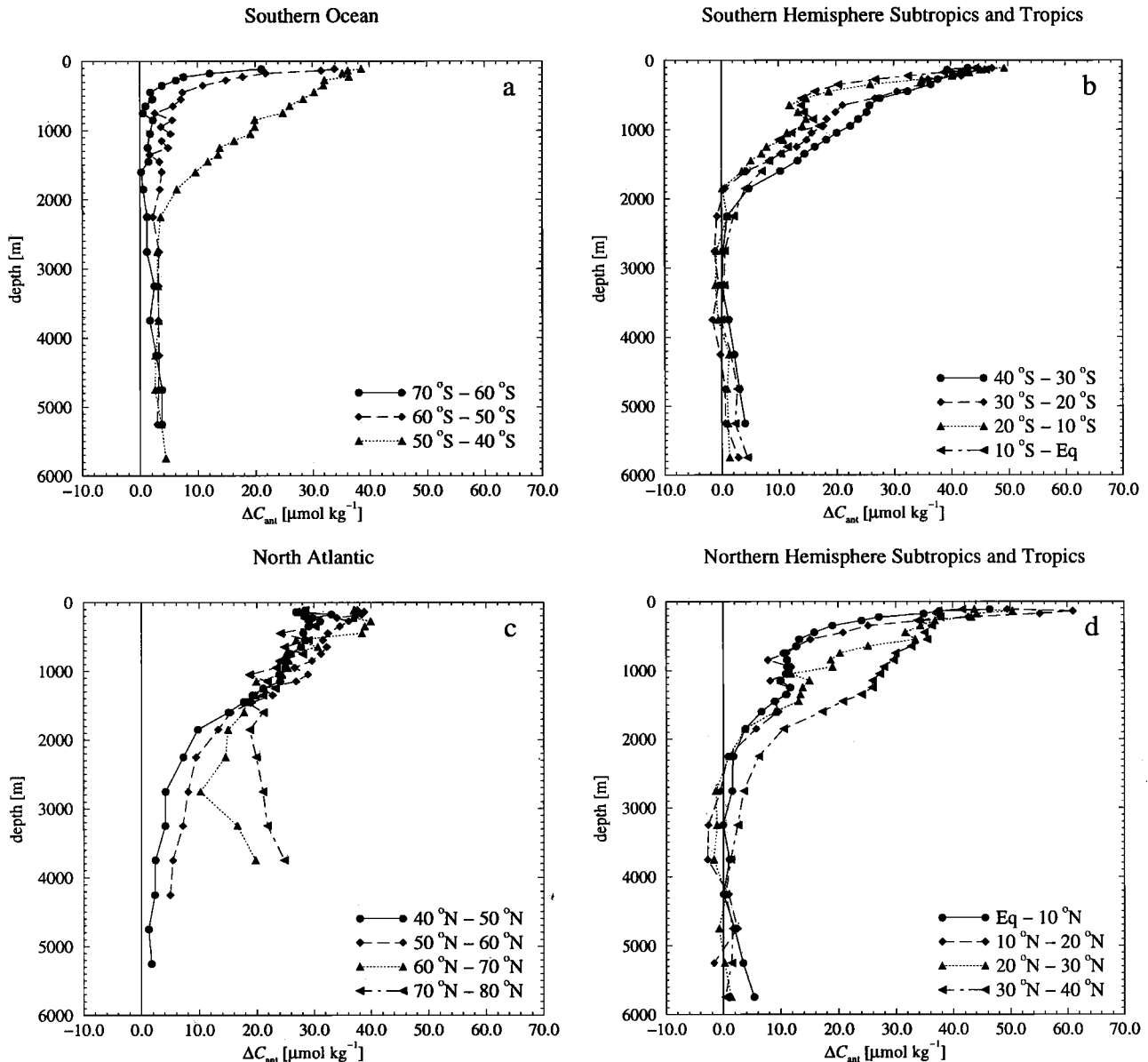
Figure 8. Horizontally averaged profiles of ΔC_{ant} in the Atlantic Ocean. (a) Profiles in 10° latitude belts from 70°S to 40°S. (b) Profiles in 10° latitude belts from 40°S to the equator. The profiles in the South Atlantic correspond to the year 1989. (c) Profiles in 10° latitude belts from the 40°N to 80°N. (d) Profiles in 10° latitude belts from the equator to 40°N. The profiles in the North Atlantic correspond to the year 1982.

North Atlantic north of 60°N, deep vertical penetration of ΔC_{ant} is found with concentrations above 10 μmol kg^{-1} down to the bottom. In sharp contrast to this the vertical penetration of anthropogenic CO₂ in the South Atlantic south of 50°S is shallow, and south of 60°S, ΔC_{ant} falls below 5 μmol kg^{-1} already at depths around 600 to 800 m. Below 800 m the concentrations are relatively constant between 2 and 5 μmol kg^{-1}.

The zonal mean distribution of ΔC_{ant} in the Atlantic Ocean is largely consistent with expectations based on the current knowledge of thermocline structure and ven-

tilation [*Rooth and Östlund*, 1972; *Sarmiento et al.*, 1982] and of the circulation of the lower limb of thermohaline overturning [*Smethie*, 1993; *Doney and Jenkins*, 1994; *Fine*, 1995]. The sharp contrast between the northern and southern high latitudes requires more discussion. The latitude belts north of 60°N comprise mainly the Greenland and Norwegian Seas. *Schlosser et al.* [1995] and *Smethie et al.*, [1986, 1988] showed that the deep waters in this region are ventilated on timescales of 10 to 40 years. The significantly higher concentration of ΔC_{ant} at middepth in the latitude belt

from 50°N to 60°N compared to the same belt in the south is caused by the southward spreading of relatively newly formed North Atlantic Deep Water (NADW) as identified from bomb-produced tritium and CFC data [Smethie, 1993; Doney and Jenkins, 1994; Fine, 1995].

However, why do the waters in the South Atlantic contain so little anthropogenic CO$_2$, although deep water formation is well known to occur in the Weddell Sea? Poisson and Chen [1987] argued that the observed low ΔC_{ant} concentrations in the deep Southern Ocean are presumably the result of three factors: the short residence time of surface waters, substantial dilution of deep and bottom waters by subsurface mixing with old waters, and effective inhibition of air-sea gas exchange by sea ice, especially during winter. This finding is also corroborated by measurements of CFCs, ^{39}Ar, and ^{14}C in the Weddell Sea and Southern Ocean [Warner and Weiss, 1992; Roether et al., 1993; Schlosser et al., 1994]. Thus the low reconstructed concentrations of ΔC_{ant} in the two southernmost latitude belts appear acceptable on the basis of what is presently known about deep and bottom water formation in the South Atlantic. Interpretation of the details in the ΔC_{ant} profiles is difficult because of the uncertainties in the separation of ΔC_{ant}.

In order to investigate the distribution of ΔC_{ant} in the Atlantic Ocean in more detail, I turn to Figure 9 which illustrates a meridional section along the western transect shown in Figure 2. ΔC_{ant} concentrations are highest in near-surface waters, and decrease steadily downward. Two distinct maxima (>50 μmol kg^{-1}) can be found in the upper 200 m in both hemispheres at approximately 20°S and 20°N associated with maxima in temperatures. The anthropogenic CO$_2$ uptake capacity of seawater is strongly temperature dependent, and waters above 25°C can contain more than 45 μmol kg^{-1} in accordance with the observations. The distribution of ΔC_{ant} in the upper waters follows more or less the vertical extent and structure of the main thermocline except in the high-latitude North Atlantic. This is well displayed by the pattern of the 30 μmol kg^{-1} isoline. The downward slope of the 10 and 20 μmol kg^{-1} isolines in the north is related to the southward spreading of relatively young NADW, which takes with it anthropogenic CO$_2$. Anthropogenic CO$_2$ is entering the deep Atlantic also from the South, but the signal is much weaker as discussed above. Only waters below 3000 m, north of 40°S and south of 40°N, contain essentially no anthropogenic CO$_2$ (< 1 μmol kg^{-1}).

The characteristics of anthropogenic CO$_2$ in the eastern Atlantic Ocean show much the same general features with some notable differences (see Figure 10). The downward and southward spreading of anthropogenic CO$_2$ at 50°N to 60°N is much smaller. Concentrations above 5 μmol kg^{-1} are found only above a depth of approximately 2000 m, whereas the 5 μmol kg^{-1} isoline

extends to the bottom at 4000 m at 50°N in the western section (Figure 9). This asymmetry is due to the lower limb of the thermohaline circulation which transports young waters southward in the deep western boundary current [Fine, 1995; Doney and Jenkins, 1994]. Along its pathway it constantly exchanges water with the interior. The deep eastern ocean is much less ventilated by young waters from the north (Figure 10). However, CFC 11 and CFC 12 data from the Oceanus 202 meridional cruise in the eastern North Atlantic along approximately 20°W [Doney and Bullister, 1992] indicate a much deeper and more southward penetration of relatively fresh waters. Penetration of the CFCs down to depths below 4000 m has been found as far south as 35°S. This indicates that this separation technique might underestimate the ΔC_{ant} concentrations in the deep eastern North Atlantic for reasons yet unknown.

Figure 11 shows a section in the South Atlantic from 60°W near the coast of South America to 20°E off the coast of South Africa. This section is not strictly zonal (see Figure 2). From 60°W to 20°W it follows approximately the 47°S latitude circle, then it turns northeastward until 30°S/4°W. It then continues eastward along 30°S. This section intersects various fronts between 20°W and 3°W [Gordon et al., 1992]: at approximately 15°W the subantarctic front, at 10°W the subtropical front, and at about 7°W the Benguela-South Atlantic Current front. The subantarctic front is intersected again at approximately 34°W. These fronts are reflected in changes in the slopes in the isolines of ΔC_{ant}. The western and eastern part of this section are therefore reflecting two different regimes: West of 20°W the section is within the Subantarctic and Polar Frontal Zones [Sievers and Nowlin, 1984], whereas east of 3°W the section represents subtropical water masses. The isolines in the middepth ocean in the western part of the section slope downward from the east to the west. The section also reveals deep penetration of ΔC_{ant} close to the South American shelf. This might be caused by the presence of Circumpolar Deep Water, which spreads northward as a deep western boundary current at a depth of about 2000 m [Reid et al., 1977]. However, the exact structure of this feature is not well defined because of low resolution of the observations. The concentrations of ΔC_{ant} in the main thermocline are very similar in the eastern part of the section (east of 3°W) despite the different thermocline structure and circulation regime. Higher concentrations are found in the near-surface waters because of the higher temperatures. Near the eastern end the section passes across one of the main upwelling centers off the coast of Africa [Gordon et al., 1992]. This causes an upward bow in the isolines in the upper waters in this region. No anthropogenic CO$_2$ is discernible below about 2000 m, in sharp contrast to the western part of the section.
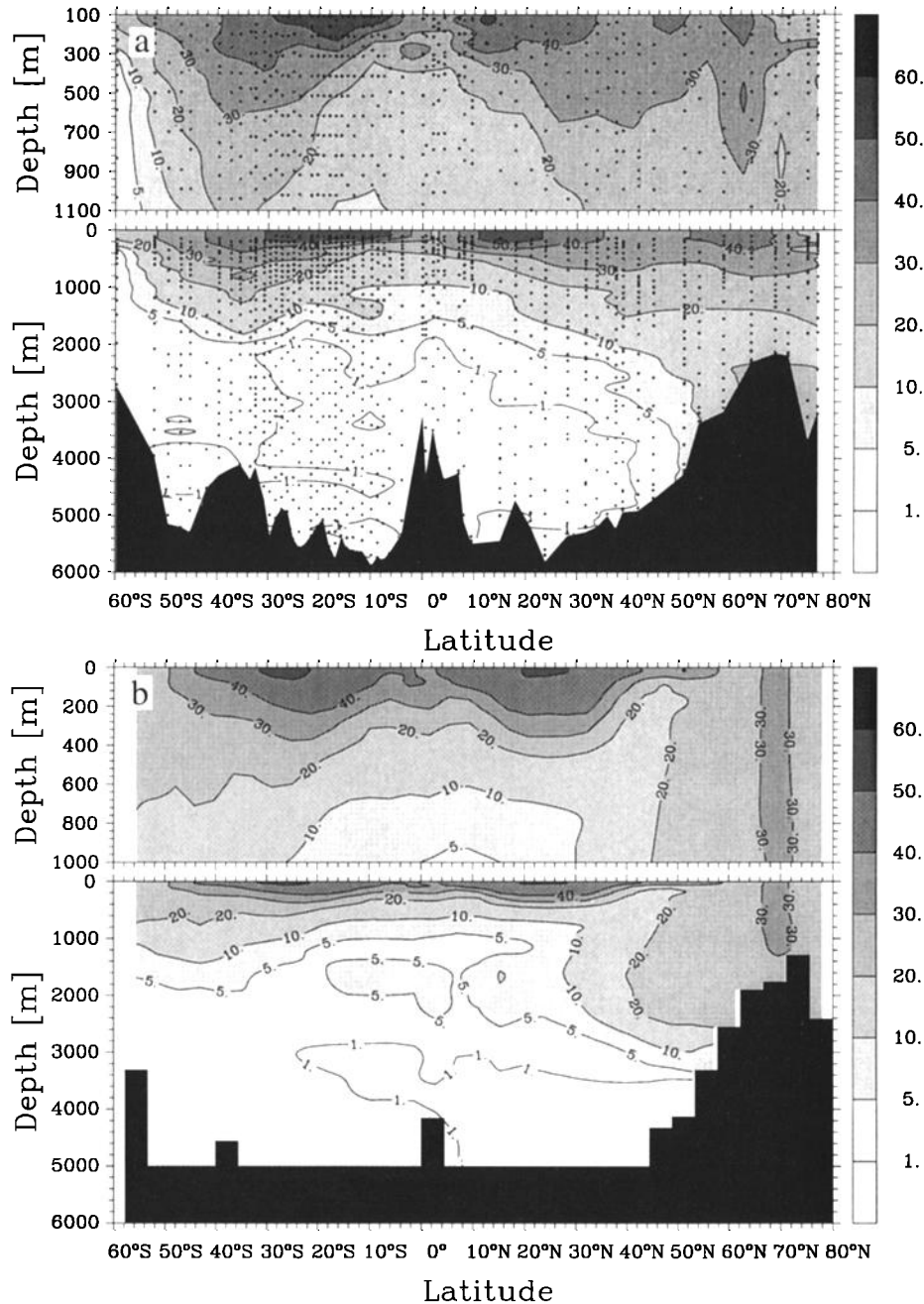
Figure 9. Meridional sections of ΔC_{ant} (micromoles per kilogram) from 60°S to 80°N in the western Atlantic Ocean. (a) Observations along the western transect shown in Figure 2. Data are from the Transient Tracers in the Oceans (TTO) North Atlantic Study (1981), the TTO Tropical Atlantic Study (1982-1983), and the South Atlantic Ventilation Experiment (1989) and refer therefore to different years in the different regions. The uncertainty in the reconstructed ΔC_{ant} has been estimated to be about 9 μmol kg^{-1}. Small circles indicate observations. (b) Results of a simulation using the Princeton ocean biogeochemistry model [*Sarmiento et al.*, 1995b] along the same transect within the resolution of the model. The model results are the average for the year 1986.

The objectively analyzed distributions of anthropogenic CO$_2$ on two isopycnal surfaces are displayed in Figures 12 and 13. These surfaces are the σ_θ 27.10 surface, which represents the Subpolar Mode Water in the face, which represents the Subpolar Mode Water in the

North Atlantic [*Kawase and Sarmiento*, 1985] and the Subantarctic Mode Water in the South Atlantic [*Sievers and Nowlin*, 1984], and the σ_2 37.00 surface, which marks the core of the NADW.
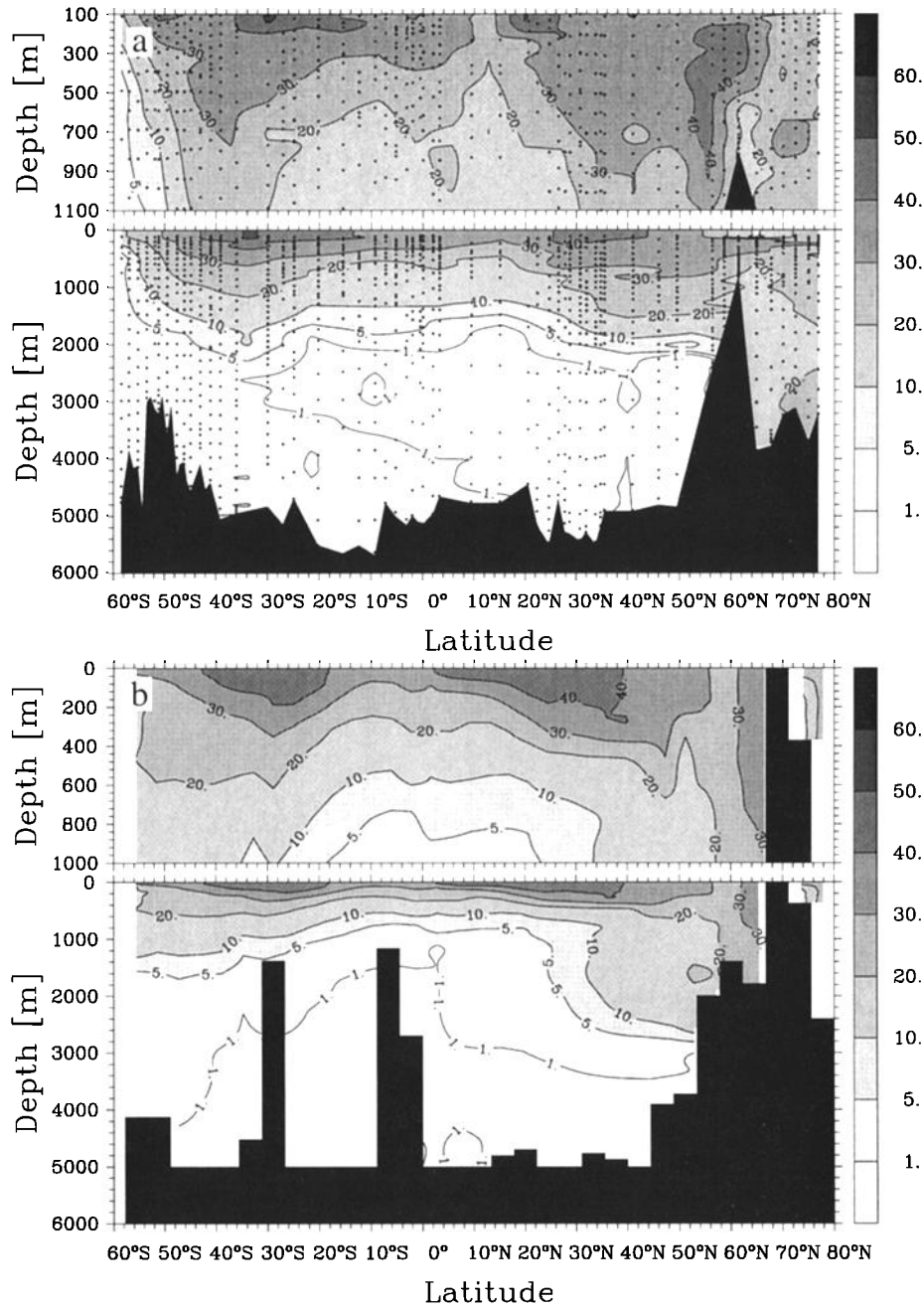
Figure 10. Meridional sections of ΔC_{ant} (micromoles per kilogram) from 60°S to 80°N in the eastern Atlantic Ocean. (a) Observations along the eastern transect shown in Figure 2. Data are from the Transient Tracers in the Oceans (TTO) North Atlantic Study (1981), the TTO Tropical Atlantic Study (1982-1983), the South Atlantic Ventilation Experiment (1989), and the *Meteor* 11/5 cruise (1991) and refer therefore to different years in the different regions. The uncertainty in the reconstructed ΔC_{ant} has been estimated to be about 9 μmol kg^{-1}. Small circles indicate observations. (b) Results of a simulation using the Princeton ocean biogeochemistry model [*Sarmiento et al.*, 1995b] along the same transect within the resolution of the model. The model results are the average for the year 1986.

On the σ_θ 27.10 surface (Figure 12), anthropogenic CO₂ shows a distinct tongue of high concentrations in the North Atlantic, extending from the outcrop in the northeast to the southwest. This reflects primarily the anticyclonic gyre transport, where anthropogenic CO₂, similar to bomb tritium, is subducted into the thermocline in the northeast [*Sarmiento et al.*, 1982]. A ΔC_{ant} front can be identified just to the south, extend-
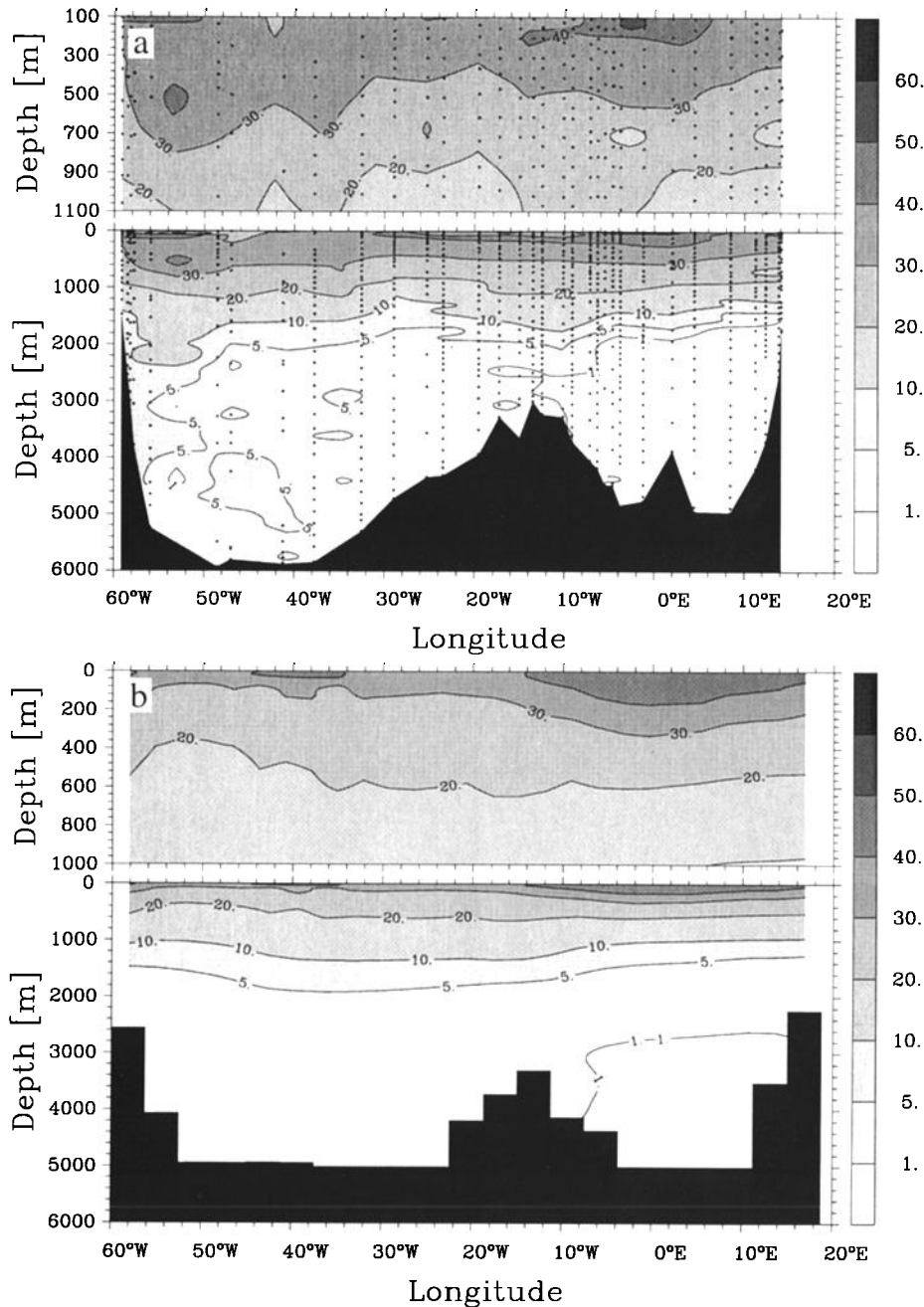
Figure 11. Zonal sections of ΔC_{ant} (micromoles per kilogram) from 60°W to 20°E in the South Atlantic Ocean. (a) Observations along the transect shown in Figure 2. Note that the section runs from 60°W to 20°W along 47°S, then turns northward until 30°S at 4°W and then runs eastward along 30°S until 16°E. Data are from the South Atlantic Ventilation Experiment (1989). The uncertainty in the reconstructed ΔC_{ant} has been estimated to be about 9 μmol kg^{-1}. Small circles indicate observations. (b) Results of a simulation using the Princeton ocean biogeochemistry model [*Sarmiento et al.*, 1995b] along the same transect within the resolution of the model. The model results are the average for the year 1989.

ing from northeastern South America across the tropical North Atlantic to the western tip of Africa at about 15°N. This front coincides with the North Equatorial Current and divides the high-salinity northern subtropical gyre waters from the low-salinity equatorial waters [*Kawase and Sarmiento*, 1985]. The invasion of anthropogenic CO$_2$ from the south is nearly uniform across the entire basin south of 20°S. A very similar pattern is displayed by the CFCs [*Warner and Weiss*, 1992] However, the CFCs show a different distribution in the
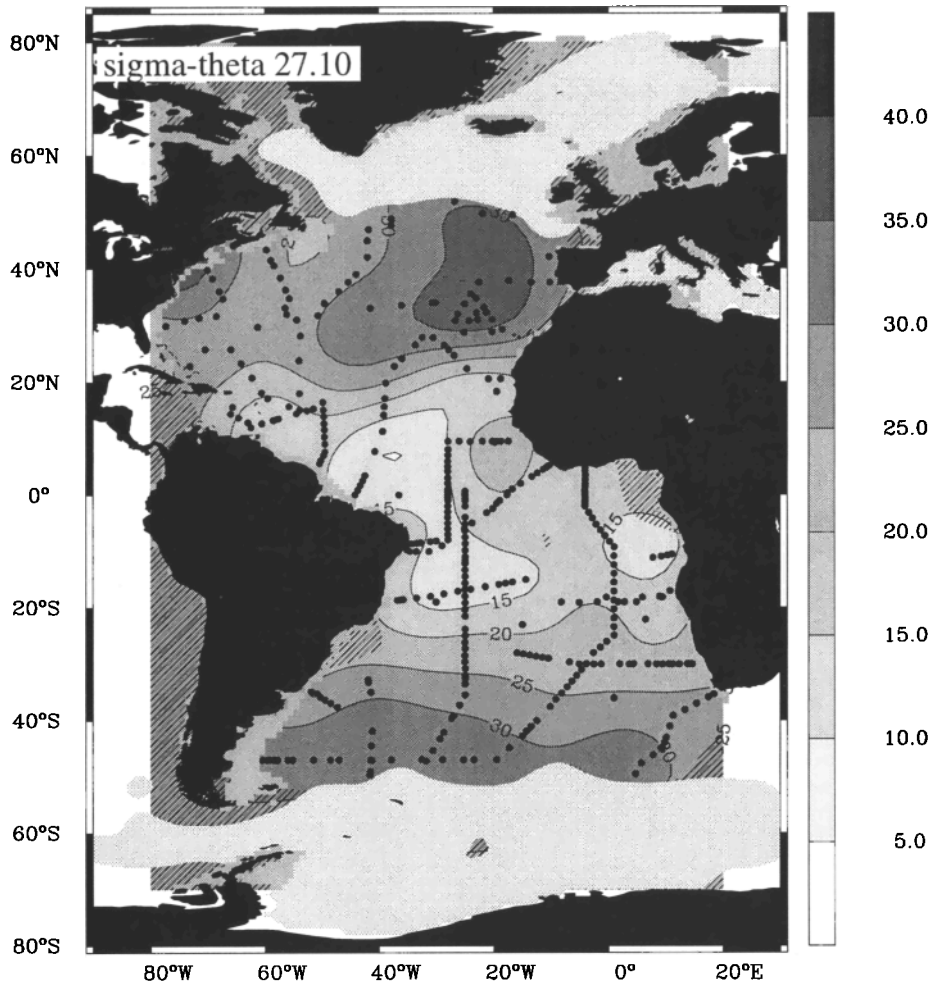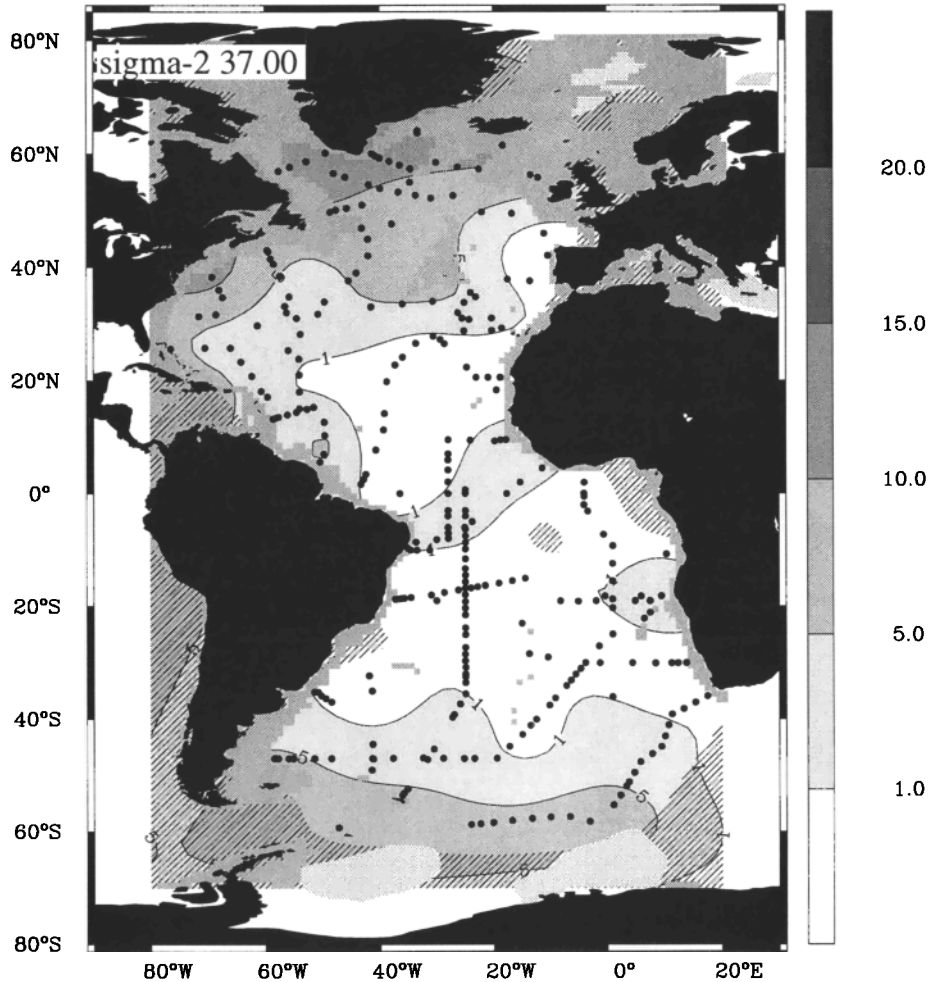
Figure 12. Objectively analyzed distribution of anthropogenic CO_2 (micromoles per kilogram) on the $\sigma_\theta = 27.10$ surface in the Atlantic Ocean. This isopycnal surface represents the Subpolar Mode Water in the north and the Subantarctic Mode Water in the south. Circles denote the stations; stippling denotes areas where the waters of this potential density are not present in wintertime (determined from the National Oceanic and Atmospheric Administration (NOAA) National Environmental Satellite and Information Service (NESDIS) atlas [*Levitus et al.*, 1994b; *Levitus and Boyer*, 1994]). Cross-hatched areas are regions where the estimated error in objectively analyzed ΔC_{ant} is greater than 5 μmol kg^{-1}.

tropical regions. *Warner and Weiss* [1992] found significantly higher concentrations in the western part of the tropical South Atlantic and found concentrations near the detection level in the east. My ΔC_{ant} data suggest the opposite. It must be emphasized, however, that the reconstruction of ΔC_{ant} in the tropical Atlantic is not very well constrained because of the few data points available to determine the tropical end-member values of ΔC_{diseq}. The CFC data indicate that I might have overestimated ΔC_{ant} in the eastern part of the tropical South Atlantic. The influence of these overestimated values on the inventory of CO_2 in the Atlantic Ocean is, however, very small, because the affected water mass

constitutes less than a percent of the total volume of the Atlantic Ocean.

The pattern of ΔC_{ant} on the σ_2 37.00 surface differs substantially in the North Atlantic from that on the shallower surface (see Figure 13). High concentrations of anthropogenic CO_2 are found in the northwestern part of the North Atlantic and extend southward along the eastern coasts of the American continents. This distribution reflects the pathway of the deep western boundary current which transports freshly formed NADW southward within decades [*Weiss et al.*, 1985; *Doney and Jenkins*, 1994; *Fine*, 1995; *Smethie*, 1993]. The eastern North Atlantic is essentially free of anthro-

Figure 13. Objectively analyzed distribution of anthropogenic CO$_2$ (micromoles per kilogram) on the $\sigma_2 = 37.00$ surface in the Atlantic Ocean. This isopycnal surface characterizes the core of the middle North Atlantic Deep Water. Circles denote the stations; stippling denotes areas where the waters of this potential density are not present in wintertime (determined from the NOAA NESDIS atlas [*Levitus et al.*, 1994b; *Levitus and Boyer*, 1994]). Cross-hatched areas are regions where the estimated error in objectively analyzed ΔC_{ant} is greater than 5 μmol kg^{-1}.

pogenic CO$_2$ on this potential density surface. The pathway of the anthropogenic CO$_2$ invasion from the south is similar to the one found on the isopycnal σ_θ 27.10. Concentrations of ΔC_{ant} above 5 μmol kg^{-1} are only found south of about 50°S.

4.4. Inventories of Anthropogenic CO$_2$

The oceanic inventory of anthropogenic CO$_2$ is estimated on the basis of TTO NAS, TTO TAS, SAVE, *Meteor* 11/5, and *Meteor* 15/3. The surveys in the North Atlantic (TTO NAS and TTO TAS) have been conducted between 1981and 1983, whereas the South Atlantic was sampled between 1987 and 1991 (SAVE, *Meteor* 11/5, and *Meteor* 15/3). In order to take this time difference into account, I calculate the inventory separately for the North and the South Atlantic. The inventory of each latitude belt is determined by vertically integrating the mean ΔC_{ant} profile in that latitude belt, taking the varying horizontal cross section area into account [see *Gruber et al.*, 1996]. Negative values of the mean ΔC_{ant} profile are set to zero in the inventory calculation. The specific inventories are then calculated by dividing the inventories by the surface area of that latitude belt. The results are shown in Table 4.

For the North Atlantic Ocean between the equator and 80°N a total inventory of 18.2×10^{14} mol C or about 21.8 Gt C (1 Gt = 10^{15} g) and a specific inventory of about 39 mol C m^{-2} was obtained. These inventories refer to 1982, the middle year of the North Atlantic cruises. The values calculated for the latitude belts from 10°N to 80°N are with the exception of the latitude belt from 10°N to 20°N identical to the inventories reported by *Gruber et al* [1996] despite the fact that the effect

Table 4. Summary of the Estimated Water Column Inventory of Anthropogenic CO_2 in the Atlantic Ocean by 10°Latitude Belts

Latitude Belt, deg	Surface Area,[a] 10^{12} m^2	Volume,[a] 10^{16} m^3	Number of Stations	Specific Inventory, mol C m^{-2}	Inventory, 10^{14} mol C	Inventory, Gt C
		South Atlantic 1989				
70°S - 60°S	4.6	1.7	19	10	0.5	0.6
60°S - 50°S	6.2	2.2	51	20	1.3	1.5
50°S - 40°S	7.5	3.1	79	46	3.4	4.1
40°S - 30°S	7.4	2.9	65	45	3.3	4.0
30°S - 20°S	6.7	2.7	80	37	2.5	3.0
20°S - 10°S	6.1	2.7	171	31	1.9	2.3
10°S - Eq	6.1	2.6	82	33	2.0	2.5
Total South Atlantic (1989)	44.8	17.9	547	33 (mean)	14.9	18.0
		North Atlantic 1982				
Eq - 10°N	6.8	2.4	70	29	1.9	2.3
10°N - 20°N	8.0	3.1	41	33	2.7	3.2
20°N - 30°N	8.9	3.6	53	40	3.6	4.3
30°N - 40°N	7.0	2.9	85	59	4.2	5.0
40°N - 50°N	5.3	1.6	26	43	2.3	2.8
50°N - 60°N	4.8	0.9	60	40	1.9	2.3
60°N - 70°N	3.7	0.4	22	28	1.0	1.2
70°N - 80°N	2.3	0.2	14	25	0.6	0.7
Total North Atlantic (1982)	46.8	15.0	371	39 (mean)	18.2	21.8

[a]Boundaries at 70°W and 20°E in the Southern Ocean.

of mixing between the different end-member ΔC_{diseq} has been taken into account explicitly in the present study. The anthropogenic CO_2 inventory in the South Atlantic Ocean from 70°S to the equator is estimated to be 14.9×10^{14} mol C or about 18.0 Gt C. The mean specific inventory of 33 mol C m^{-2} is significantly lower than in the North Atlantic. The South Atlantic inventories are representative for 1989, the middle year of the South Atlantic cruises. *Gruber et al.* [1996] estimated the error of these inventories to be about 20% based on the signal-to-noise ratio of ΔC_{ant}. I refined their analysis by performing an error propagation calculation using the same uncertainties in the measured quantities and ratios as *Gruber et al.* [1996]. This yields an uncertainty in the inventories of about 7% to 9% (1.9 Gt C for the North Atlantic and 1.3 Gt C for the South Atlantic). This calculation assumes that all errors are uncorrelated and of random origin. However, systematic errors can have a profound effect on the estimated inventory. In order to address this possibility, two cases were investigated wherein the stoichiometric carbon to oxygen ratio during remineralization $r_{C:O_2}$ has been set to the upper limit (-0.780) and lower limit (-0.596) of the uncertainty given by *Anderson and Sarmiento* [1994]. The former corresponds approximately to Refield's ratio of 106 to -138 [*Redfield et al.*, 1963], whereas the latter corresponds roughly to a stoichiometry of 117 to -196. The choice of these two scenarios is based on the fact

that the largest uncertainty in the separation technique is associated with this ratio, especially in waters having high apparent oxygen utilization [*Gruber et al.*, 1996]. The Atlantic inventories increase by about 8 Pg C (20%) in the case of $r_{C:O_2} = -0.596$, whereas the inventories decrease by only about 3 Pg C (8%) in the Redfield case. The changes are larger in the South Atlantic than in the North Atlantic, since the apparent oxygen utilization is on average higher south of the equator. A systematic bias in $r_{C:O_2}$ of this magnitude is unlikely, but other systematic errors might confound the estimated ΔC_{ant}. Especially, a possible uncertainty of ± 2 μmol kg^{-1} in the deep ocean ΔC_{diseq} could over 3000 m add up to about 6 mol m^{-2}, which is equivalent to approximately 20% of the total water column inventory. I therefore continue to assume that the errors of the inventories are of the order of 20% with most of the uncertainty stemming from possible systematic biases. It must be noted, however, that the magnitude of this error is only a rough estimate, and more refined techniques are necessary in order to obtain improved estimates of this error.

The distribution of the specific inventories by latitude belt is shown in Figure 14. The highest specific inventories are found in the subtropical regions of both hemispheres between 30° and 40°. The maximum in the North Atlantic is somewhat larger (56 mol C m^{-2}) than the South Atlantic maximum (49 mol C m^{-2}). The tropics and the high latitudes have significantly lower
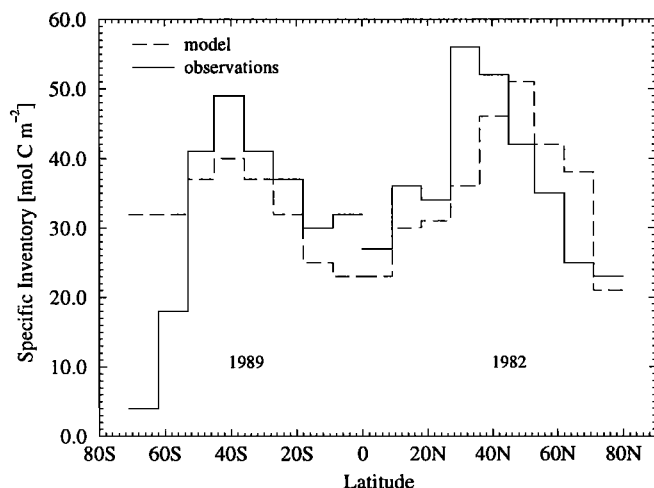
Figure 14. Specific inventories of anthropogenic CO_2 in the Atlantic Ocean. The model based inventories are from the Princeton ocean biogeochemistry model [*Sarmiento et al.* 1995b]. North of the equator the inventories refer to the year 1982; south of the equator they refer to the year 1989.

specific inventories. This distribution reflects the wind-driven meridional circulation [*Sarmiento et al.*, 1992]. Ekman divergence near the equator and in the temperate regions causes anthropogenic CO_2 which entered the ocean in these regions to be laterally transported toward the subtropics. Anthropogenic CO_2 accumulates then in the subtropical convergence zone causing high specific inventories. A very similar pattern is observed for other transient tracers like bomb radiocarbon [*Broecker et al.*, 1995] and CFCs [*Doney and Bullister*, 1992]. In the northern high latitudes the specific inventories are relatively small despite the fact that anthropogenic CO_2 has penetrated to the bottom. This is primarily due to the shallowness of the ocean north of 60°N. The specific inventories south of 50°S are very low, reflecting the very shallow vertical penetration of anthropogenic CO_2 as displayed in Figure 8 and discussed in section 4.3. The relative uncertainties of the specific inventories in the two southernmost belts are high, however, because of the large relative uncertainties associated with the near zero concentrations in the middepth and deep waters.
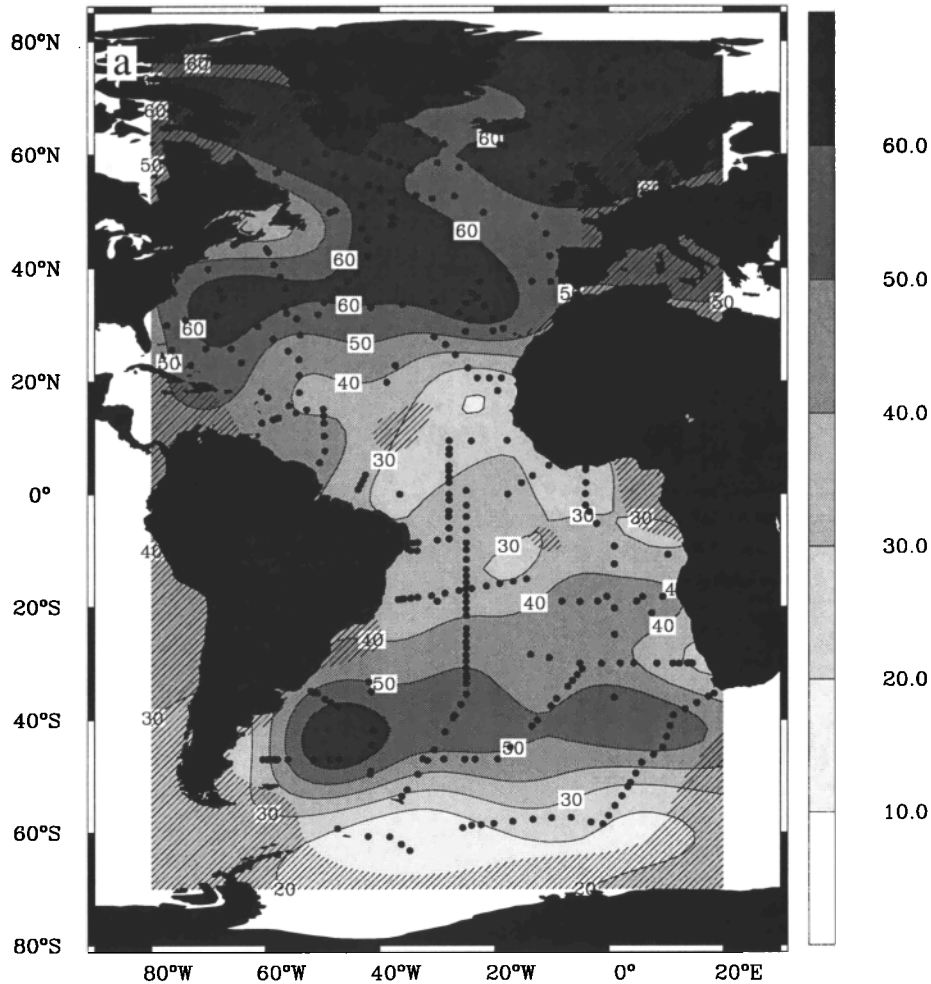
Figure 15a shows the objectively analyzed distribution of the vertically integrated ΔC_{ant} concentrations at each station. This quantity is not identical to the specific inventory because of topographic effects. The difference is particularly relevant when ΔC_{ant} has nearly vertically uniform concentrations as found in the Greenland and Norwegian Seas. Here the vertical integral of ΔC_{ant} for a specific station is primarily determined by the depth. Since oceanographic stations are preferably located in the deeper parts of a basin, the mean value

of the vertically integrated ΔC_{ant} over a larger region is greater than the mean specific inventory in this region. This explains the apparent discrepancy in the high-latitude North Atlantic between Figures 14 and 15a. South of 60°N the difference between the vertically integrated ΔC_{ant} and the specific inventory of ΔC_{ant} is small, and both quantities show similar large-scale features. High vertically integrated ΔC_{ant} values (> 50 mol C m^{-2}) are found in the entire North Atlantic north of 30°N. Decreasing values toward the continents and between Europe and Greenland are caused by shoaling depths. A distinct front running from South America across the tropical Atlantic to the western tip of Africa separates the low vertically integrated concentrations in the equatorial Atlantic from the higher values to the north. In the western Atlantic this front is identical to the front described above in Figure 12, shown to be associated with the North Equatorial Current. In the eastern basin the isolines bend to the south because of the contribution of the southward spreading western boundary current in the deeper layers. The vertically integrated ΔC_{ant} values show a broad band of higher values in the subtropical South Atlantic. The maximum value of vertically integrated ΔC_{ant} in the South Atlantic is found in the eastern portion of the South Atlantic subtropical gyre, consistent with expectations. Vertically integrated ΔC_{ant} decreases rapidly south of 55°S. Lower values toward the continents are again due to the shoaling topography.

4.5. Model Comparison

I compare my estimates of anthropogenic CO_2 in the Atlantic Ocean with the results of the Princeton ocean biogeochemistry model (POBM) [*Sarmiento et al.*, 1995b] . This model s a global coarse-resolution model based on the non seasonal circulation model of *Toggweiler et al.* [1989a]. A full natural carbon cycle is included, representing the solubility pump, the soft-tissue pump, and the carbonate pump. This model has been spun up to a preindustrial steady state with an atmospheric CO_2 concentration of 280 μatm. The uptake simulation starts in 1767. Atmospheric CO_2 is prescribed by the same smoothed spline fit through atmospheric CO_2 data as used for the calculation of ΔC_t^*. Model results which pertain to the entire Atlantic are analyzed for the year 1986. In the other cases, results from 1982 are used in the North Atlantic and are used from 1989 in the South Atlantic.

The POBM predicts anthropogenic CO_2 inventories of 20.0 Gt C (North Atlantic, 1982) and 17.7 Gt C (South Atlantic, 1989), in very good agreement with my reconstruction based on observations (see Tables 5 and 6). The global uptake rate of the POBM between 1982 and 1989 is about 2 Gt C yr^{-1}. This leads to an increase in the total ocean inventory from 106 Gt

Figure 15. (a) Objectively analyzed distribution of the vertically integrated concentrations of ΔC_{ant} (moles C per square meter). The observations refer to the years from 1981 to 1983 in the North Atlantic and refer to the years from 1987 to 1991 in the South Atlantic. Circles denote stations, and the hatched pattern denotes the regions where the error of the objective interpolation is greater than 5 mol C m^{-2}. (b) Distribution of the vertically integrated concentration of ΔC_{ant} in the Princeton ocean biogeochemistry model [*Sarmiento et al.* 1995b] for the year 1986 (moles C per square meter).

C in 1982 to 120 Gt C in 1989. About 34% of the oceanic uptake of anthropogenic CO₂ occurs in the Atlantic ocean, which covers only about 26% of the total ocean surface. This enhanced uptake by the Atlantic is mainly due to the North Atlantic, where deep water formation and strong vertical overturning enhance the surface-to-deep ocean transport. This transport is the main controlling factor for the oceanic uptake of anthropogenic CO₂ [*Siegenthaler and Joos*, 1992; *Sarmiento et al*, 1992]. The POBM is known to have a too sluggish thermocline ventilation and a much too diffusive thermocline [*Toggweiler et al.*, 1989b; *Sarmiento et al.*, 1992]. Obviously, these deficiencies seem not to have a large impact on the anthropogenic CO₂ uptake on the large scale.

For a more detailed comparison of the model results with our reconstruction I return to Figures 9 - 11. The

model shows good qualitative agreement in both the western (Figure 9) and eastern (Figure 10) meridional sections. However, substantial deviations occur, especially in the North Atlantic. The model underpredicts the concentrations in the main thermocline of the subtropical to temperate regions. The isolines lie between 200 and 400 m too shallow compared to observations. A particularly large deficiency shows up in the POBM between 40°N and 50°N at depths between 200 and 500 m as already discussed by *Gruber et al.* [1996] This deficiency has been attributed to the artificial upwelling of deep water with low concentrations of ΔC_{ant} on the landward side of the Gulf Stream [*Toggweiler et al.*, 1989b, p. 8249]. This upwelling is caused by the strictly horizontal orientation of lateral mixing in the POBM [*Veronis*, 1975]. Rotation of the diffusion tensor to create isopycnal/diapycnal mixing has been
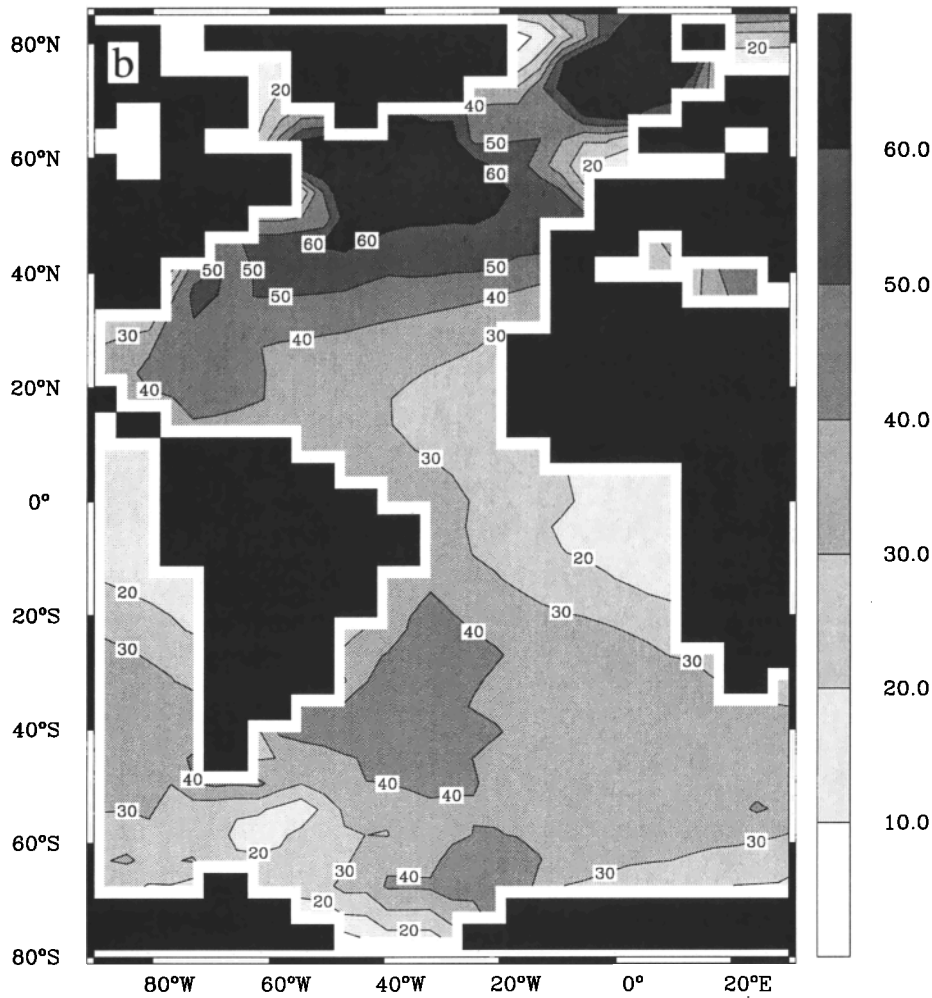
Figure 15. (continued)

shown to reduce this artificial upwelling [*Gough and Lin*, 1995]. However, *Duffy et al.* [1995a] still found an eastward displacement of the maximum specific inventory of bomb radiocarbon, indicative of the Veronis effect, when employing a z level model similar to the one employed here but with isopycnal/diapycnal mixing. *Follows and Marshall* [1996] proposed that eddy transport, which is not explicitly included in such coarse-resolution models, may also play an important role

The POBM simulates the downward depression of the isolines in the northern high latitudes due to the southward spreading of NADW. However, the simulated NADW does not penetrate below 3000 m [*Toggweiler et al.*, 1989a], since denser waters of Antarctic origin fill up the entire deep North Atlantic. The model overpredicts the ΔC_{ant} concentrations in the NADW, partially compensating the deficiency in the upper thermocline. Both model and observations predict very low concentrations in the deep and bottom waters in the South Atlantic A large difference exists, however, in the up-

per waters south of 40°S. The observations indicate a substantial shoaling of the isolines toward the south, whereas the model simulates much deeper penetration at these latitudes. The POBM is known to have excessive convection in the Southern Ocean and to produce deep waters which are too young compared to observations [*Toggweiler et al.*, 1989b]. The introduction of a parameterization of the effects of mesoscale eddies not resolved by coarse-resolution models [*Gent and McWilliams*, 1990; *Gent et al.*, 1995] has been shown to dramatically reduce convective adjustment and to improve the simulation of temperature, salinity, radiocarbon and CFCs in the intermediate and deep Southern Ocean [*Danabasoglu et al.*, 1994; *England*, 1995; *Duffy et al.*, 1995b; *Robitaille and Weaver*, 1995; *Hirst and McDougall*, 1996; *Duffy et al.*, 1997].

The too low concentrations of ΔC_{ant} in the thermocline from 40°S to 40°N are also evident in a more detailed comparison between the model predicted and observed specific inventories (Table 5 and Figure 14). The model underpredicts the specific inventories in these lat-

Table 5. Comparison of the Estimated Water Column Inventory of Anthropogenic CO_2 in the Atlantic Ocean With Estimates From the Princeton Ocean Biogeochemistry Model (POBM) [*Sarmiento et al.*, 1995b] for the Years 1982 and 1989 by Latitude Belt

Latitude Belt	POBM			Observations		
	Surface Area,[a] 10^{12} m^2	Inventory, Gt C	Specific Inventory, mol C m^{-2}	Surface Area,[b] 10^{12} m^2	Inventory, Gt C	Specific Inventory, mol C m^{-2}
South Atlantic 1989						
71°S - 62°S	3.9	1.5	32	3.4	0.2	4
62°S - 53°S	5.3	2.0	32	5.2	1.1	18
53°S - 45°S	6.4	2.8	37	6.3	3.1	41
45°S - 36°S	6.9	3.3	40	6.9	4.0	49
36°S - 27°S	6.3	2.8	37	6.5	3.2	41
27°S - 18°S	5.7	2.2	32	5.9	2.6	37
18°S - 9°S	5.2	1.6	25	5.5	2.0	30
9°S - Eq	5.3	1.5	23	5.6	2.1	32
Total South Atlantic (1989)	45.0	17.7	33 (mean)	45.3	18.3	33 (mean)
North Atlantic 1982						
Eq - 9°N	5.7	1.6	23	6.1	2.0	27
9°N - 18°N	6.8	2.4	30	7.0	3.0	36
18°N - 27°N	8.0	3.0	31	8.0	3.3	34
27°N - 36°N	7.1	3.1	36	7.0	4.7	56
36°N - 45°N	5.4	3.0	46	5.5	3.4	52
45°N - 53°N	4.1	2.5	51	4.0	2.0	42
53°N - 62°N	4.4	2.2	42	4.8	2.0	35
62°N - 71°N	3.1	1.4	38	2.8	0.8	25
71°N - 80°N	3.3	0.8	21	1.8	0.5	23
Total North Atlantic (1982)	47.9	20.0	35 (mean)	47.0	21.7	39 (mean)

[a]Boundaries at 67.5°W and 22.5°E in the Southern Ocean.
[b]Boundaries at 70°W and 20°E in the Southern Ocean.

Table 6. Comparison of the Total Estimated Water Column Inventory of Anthropogenic CO_2 in the Atlantic Ocean With Estimates from the Princeton Ocean Biogeochemistry Model (POBM) [*Sarmiento et al.*, 1995b]

	Global Uptake Rate, Gt C yr^{-1}	Global Inventory, Gt C	North Atlantic Inventory,[a] Gt C	South Atlantic Inventory,[b] Gt C
1982				
Observations (this study)			22 ± 5	
POBM	1.86	106	20.0	15.8
1989				
Observations (this study)				18 ± 4
POBM	2.21	120	22.7	17.7

[a]Atlantic Ocean between equator and 80°N.
[b]Atlantic Ocean between 71°S and equator.

itude belts on average by about 5 mol C m^{-2}. This is compensated by an overprediction in the Southern Ocean and in the middle to high-latitude North Atlantic, resulting in a good agreement in the total basin-wide inventories. Particularly large is the overprediction of the model south of 53°S, where the POBM simulates specific inventories of the order of 30 mol C m^{-2}, whereas my reconstruction from observations indicates specific inventories of the order of 10 mol C m^{-2}. Even taking into account the large relative error of the latter estimate (probably about 50%), the difference remains significant.

The POBM simulated distribution of the vertically integrated ΔC_{ant} concentration shows the success and deficiency of the model in even more detail (Figures 15a and 15b). The artificial upwelling in the North Atlantic displaced the maximum toward the north and east. The vertically integrated values are lower throughout the subtropical and equatorial Atlantic but significantly higher in the Southern Ocean.

4.6. Comparison With Chen's Estimates

Chen [1993] recently summarized all of his calculations and attempted to estimate a global inventory of anthropogenic CO$_2$ in the oceans. He reported for the year 1973 an inventory of 21.5 ± 4.5 Gt C in the North Atlantic (equator to 65°N) and 12.0 ± 2.5 Gt C in the South Atlantic. Both values are based on an earlier study [*Chen*, 1982]. He also presented an inventory of 0.85 ± 0.2 Gt C for the Greenland and Norwegian Seas for the year 1982 making use of the study of *Chen et al.* [1990]. His North Atlantic inventory up to 65°N is substantially larger than the inventory predicted by the POBM for the same year (15.2 Gt C), whereas good agreement is found for the South Atlantic (13.7 Gt C). Accepting the model-calculated increase of 2.5 Gt for the North Atlantic between 1973 and 1982 and adding the estimate of *Chen* [1993] for the Greenland and Norwegian Seas, an inventory of about 25 ± 5 Gt C is inferred from Chen's estimate for the entire North Atlantic (equator to 80°N) for the year 1982. This is somewhat larger than my estimate of 22 ± 5 Gt C but is well within the uncertainties. Adding the model-predicted increase of 4 Gt C for the South Atlantic between 1973 and 1989, I estimate from Chen's data a South Atlantic inventory of about 16 ± 3 Gt C for the year 1989. This is smaller than my estimate of 18 ± 4 Gt C but again is in agreement within the uncertainties.

5. Summary and Conclusions

The method of *Gruber et al.* [1996] was extended and applied to data from the North and South Atlantic sampled as part of the TTO NAS, TTO TAS, SAVE, *Meteor* 11/5, and *Meteor* 15/3 cruises. The extension of the method includes the explicit treatment of mixing between the air-sea disequilibria of the different end-members on a potential density surface. The reconstructed distribution of anthropogenic CO$_2$ in the Atlantic Ocean reflects the patterns of the oceanic uptake and subsequent redistribution of anthropogenic CO$_2$ within the ocean. Concentrations of anthropogenic CO$_2$ in the upper waters are highest in the subtropics and decrease toward the poles because of the temperature dependence of the CO$_2$ thermodynamic system. Concentrations decrease gradually with depth. Vertical penetration (5 μmol kg^{-1} front) is shallow in the tropics (1500 m) and in the Southern Ocean (700 m), intermediate in the subtropics (2000 m), and high in the high-latitude North Atlantic, where anthropogenic CO$_2$ has even reached the bottom (4000 m). This pattern reflects the ventilation of the main thermocline, the processes of deep water formation, and the flow patterns of the lower limb of the thermohaline circulation. I estimate for the entire North Atlantic (equator to 80°N) an anthropogenic CO$_2$ inventory of 22 ± 5 Gt C for the year 1982. The estimate from 10°N to 80°N is almost identical to the previous assessment of *Gruber et al.* [1996] despite the consideration of mixing in the present study. The inventory of ΔC_{ant} in the South Atlantic is estimated to be 18 ± 4 Gt C for 1989. I compared my estimates with the results of the Princeton ocean biogeochemistry model. The agreement of the total inventory in the two basins for the respective years (North Atlantic: 20.0 Gt C; South Atlantic: 17.7 Gt C) is excellent. Substantial differences, however, exist on a regional scale. Most of theses differences are related to known deficiencies in the circulation model.

Nevertheless, despite these regional discrepancies the agreement between the POBM results and my estimates on the basin scale is encouraging and suggests that the simulation of the global uptake of this model should be quite realistic. In order to test this hypothesis, it is necessary to extend this method to the global scale. This will become possible when carbon and other tracer data from the ongoing World Ocean Circulation Experiment (WOCE) will become available in the near future. First assessments of anthropogenic CO$_2$ using data from the Indian Ocean WOCE program [*Sabine et al.*, 1997] show promising results.

References

Anderson, L. A., and J. L. Sarmiento, Redfield ratios of remineralization determined by nutrient data analysis, *Global Biogeochem. Cycles, 8*(1), 65–80, 1994.

Brewer, P. G., Direct observation of the oceanic CO$_2$ increase, *Geophys. Res. Lett., 5*(12), 997–1000, 1978.

Brewer, P. G., W. S. Broecker, W. J. Jenkins, P. B. Rhines, C. G. Rooth, J. H. Swift, T. Takahashi, and R. T. Williams, A climate freshening of the deep Atlantic north of 50°N over the past 20 years, *Science, 222*, 1237–1239, 1983.

Brewer, P. G., A. Bradshaw, and R. Williams, Measurements of total carbon dioxide and alkalinity in the North Atlantic ocean in 1981, in *The Changing Carbon Cycle, A Global Analysis*, edited by J. Trabalka and D. Reichle, pp. 358–381, Springer-Verlag, New York, 1986.

Broecker, W. S., 'NO', a conservative water-mass tracer, *Earth Planet. Sci. Lett., 23*, 100–107, 1974.

Broecker, W. S., Chemical signatures associated with the freshening of northern Atlantic waters between 1972 and 1982, North Atlantic Deep Water Formation, *NASA Conf. Publ., 2367*, 13–17, 1985.

Broecker, W. S., and T. H. Peng, Gas exchange rates between air and sea, *Tellus, 26*, 21–35, 1974.

Broecker, W. S., T. H. Peng, G. Ostlund, and M. Stuiver, The distribution of bomb radiocarbon in the ocean, *J. Geophys. Res., 90*(4), 6953–6970, 1985a.

Broecker, W. S., T. Takahashi, and T.-H. Peng, Reconstruction of past atmospheric CO$_2$ from the chemistry of the contemporary ocean: An evaluation, *Tech. Rep. TRO 20*, U.S. Dep. of Energy, Washington, D. C., 1985b.

Broecker, W. S., S. Blanton, W. M. Smethie, and G. Ostlund, Radiocarbon decay and oxygen utilization in the deep Atlantic Ocean, *Global Biogeochem. Cycles, 5*(1), 87–117, 1991.

Broecker, W. S., S. Sutherland, W. Smethie, T.-H. Peng, and G. Ostlund, Oceanic radiocarbon: Separation of the natural and bomb components, *Global Biogeochem. Cycles, 9*(2), 263–288, 1995.

Chen, C.-T. A., On the distribution of anthropogenic CO$_2$ in the Atlantic and Southern Oceans, *Deep Sea Res., Part A, 29*(5), 563–580, 1982.

Chen, C.-T. A., The oceanic anthropogenic CO$_2$ sink, *Chemosphere, 27*(6), 1041–1064, 1993.

Chen, C.-T. A., and F. J. Millero, Gradual increase of oceanic CO$_2$, *Nature, 277*, 205–206, 1979.

Chen, C.-T. A., and R. M. Pytkowicz, On the total CO$_2$-titration alkalinity oxygen system in the Pacific Ocean, *Nature, 281*, 362–365, 1979.

Chen, C.-T. A., E. P. Jones, and K. Lin, Wintertime total carbon dioxide measurements in the Norwegian and Greenland Seas, *Deep Sea Res., Part A, 37*(9), 1455–1473, 1990.

Chen, C.-T. A., S.-L. Wang, and A. S. Bychkov, Carbonate chemistry of the Sea of Japan, *J. Geophys. Res., 100*(7), 13737–13745, 1995.

Chipman, D., T. Takahashi, D. Breger, and S. Sutherland, Carbon dioxide, hydrographic, and chemical data obtained during the R/V *Meteor* cruise 11/5 in the South Atlantic and Northern Weddell Sea areas (WOCE sections A-12 and A-21), *Data Rep. ORNL/CDIAC-55; NDP-045*, Carbon Dioxide Inf. Anal. Cent., Oak Ridge Natl. Lab., Oak Ridge, Tenn., 1994.

Coles, V. J., M. S. McCartney, D. B. Olson, and W. M. Smethie, Changes in Antarctic Bottom Water properties in the western South Atlantic in the late 1980s, *J. Geophys. Res., 101*(4), 8957–8970, 1996.

Danabasoglu, G., J. C. McWilliams, and P. R. Gent, The role of mesoscale tracer transports in the global ocean circulation, *Science, 264*, 1123–1126, 1994.

Dickson, A. G., Thermodynamics of the dissociation of boric acid in synthetic seawater from 273.15 to 318.15 K, *Deep Sea Res., Part A, 37*(5), 755–766, 1990.

Dickson, A. G., and J. P. Riley, The estimation of acid dissociation constants in seawater media from potentiometric titrations with strong base, II, The dissociation of phosphoric acid, *Mar. Chem., 7*, 101–109, 1979.

Doney, S. C., and J. L. Bullister, A chlorofluorocarbon section in the eastern North Atlantic, *Deep Sea Res., Part A, 39*(11/12), 1857–1883, 1992.

Doney, S. C., and W. Jenkins, Ventilation of the deep western boundary current and abyssal western North Atlantic: Estimates from tritium and ^{3}He distributions, *J. Phys. Oceanogr., 24*, 638–659, 1994.

Doney, S. C., W. J. Jenkins, and J. L. Bullister, A comparison of ocean tracer dating techniques on a meridional section in the eastern North Atlantic, *Deep Sea Res., Part I, 44*(4), 603–626, 1997.

Duffy, P. B., D. E. Eliason, A. J. Bourgeois, and C. C. Covey, Simulation of bomb radiocarbon in two global ocean general circulation models, *J. Geophys. Res., 100*(11), 22545–22563, 1995a.

Duffy, P. B., P. Eltgroth, A. J. Bourgeois, and K. Caldeira, Effect of improved subgrid scale transport of tracers on uptake of bomb radiocarbon in the GFDL ocean general circulation model, *Geophys. Res. Lett., 22*(9), 1065–1068, 1995b.

Duffy, P. B., K. Caldeira, J. Selvaggi, and M. I. Hoffert, Effects of subgrid-scale mixing parameterizations on simulated distribution of natural ^{14}C, temperature, and salinity in a three-dimensional ocean general circulation model, *J. Phys. Oceanogr., 27*, 498–523, 1997.

England, M., Using chlorofluorocarbons to assess ocean climate models, *Geophys. Res. Lett., 22*(22), 3051–3054, 1995.

Enting, I. G., C. M. Trudinger, and R. J. Francey, A synthesis inversion of the concentration and δ^{13}C of atmospheric CO$_2$, *Tellus, Ser. B., 47*, 35–52, 1995.

Fine, R. A., Tracers, time scales, and the thermohaline circulation: The lower limb in the North Atlantic ocean, *U.S. Natl. Rep. Int. Union Geod. Geophys. 1991-1994, Rev. Geophys., 33*, 1353–1365, 1995.

Fink, R., Zur Kohlenstoffchemie des Ozeans und zur Modellierung des natürlichen Kohlenstoffkreislaufes, Ph.D. thesis, Phys. Inst., Univ. of Bern, Bern, Switzerland, 1996.

Follows, M. J., and J. C. Marshall, On models of bomb ^{14}C in the North Atlantic, *J. Geophys. Res., 101*(10), 22577–22582, 1996.

Gent, P. R., and J. C. McWilliams, Isopycnal mixing in ocean circulation models, *J. Phys. Oceanogr., 20*, 150–155, 1990.

Gent, P. R., J. Willebrand, T. J. McDougall, and J. C.

McWilliams, Parameterizing eddy-induced tracer transports in ocean circulation models, *J. Phys. Oceanogr., 25*, 463–474, 1995.

Gordon, A. L., R. F. Weiss, W. M. Smethie, and M. J. Warner, Thermocline and intermediate water communication between the South Atlantic and Indian Oceans, *J. Geophys. Res., 97*(5), 7223–7240, 1992.

Gough, W. A., and C. A. Lin, Isopycnal mixing and the Veronis effect in an ocean general circulation model, *J. Mar. Res., 53*, 189–199, 1995.

Goyet, C., and P. G. Brewer, Biochemical properties of the oceanic carbon cycle, in *Modeling Oceanic Climate Interactions*, edited by J. Willebrand and D. L. T. Anderson, pp. 271–297, Springer-Verlag, New York, 1993.

Goyet, C., and A. Poisson, New determination of carbonic acid dissociation constants in seawater as a function of temperature and salinity, *Deep Sea Res., Part A, 36*(11), 1635–1654, 1989.

Gruber, N., and J. L. Sarmiento, Global patterns of marine nitrogen fixation and denitrification, *Global Biogeochem. Cycles, 11*(2), 235–266, 1997.

Gruber, N., J. L. Sarmiento, and T. F. Stocker, An improved method for detecting anthropogenic CO₂ in the oceans, *Global Biogeochem. Cycles, 10*(4), 809–837, 1996.

Heimann, M., and E. Maier-Reimer, On the relations between the oceanic uptake of CO₂ and its carbon isotopes, *Global Biogeochem. Cycles, 10*(1), 89–110, 1996.

Hirst, A. C., and T. J. McDougall, Deep-water properties and surface buoyancy flux as simulated by a z-coordinate model including eddy-induced advection, *J. Phys. Oceanogr., 26*, 1320–1343, 1996.

Houghton, J. T., L. M. Filho, B. A. Callander, N. Harris, A. Kattenberg, and K. Maskell, *Climate Change 1995: The Science of Climate Change*, Intergov. Panel on Clim. Change, Cambridge, England, 1996.

Jenkins, W. J., ³H and ³He in the Beta Triangle: Observations of gyre ventilation and oxygen utilization rates, *J. Phys. Oceanogr., 17*, 763–783, 1987.

Johnson, K. M., D. W. R. Wallace, R. J. Wilke, and C. Goyet, Carbon dioxide, hydrographic and chemical data obtained during the R/V *Meteor* cruise 15/3 in the South Atlantic ocean (WOCE section A9, February-March 1991), *Data Rep. ORNL/CDIAC-82; NDP-051*, Carbon Dioxide Inf. Anal. Cent., Oak Ridge Natl. Lab., Oak Ridge, Tenn., 1995.

Kawase, M., and J. L. Sarmiento, Nutrients in the Atlantic thermocline, *J. Geophys. Res., 90*(5), 8961–8979, 1985.

Keeling, C. D., and T. P. Whorf, Atmospheric CO₂ records from sites in the SIO air sampling network, in *Trends '93: A Compendium of Data on Global Change*, edited by T. Boden et al., *Rep. ORNL/CDIAC-65*, pp. 16–26, Carbon Dioxide Inf. Anal. Cent., Oak Ridge Natl. Lab., Oak Ridge, Tenn., 1994.

Keeling, R. F., and S. R. Shertz, Seasonal and interannual variations in atmospheric oxygen and implications for the global carbon cycle, *Nature, 358*, 723–727, 1992.

Ledwell, J. R., A. J. Watson, and C. S. Law, Evidence for slow mixing across the pycnocline from an open-ocean tracer-release experiment, *Nature, 364*, 701–703, 1993.

LeTraon, P. Y., A method for optimal analysis of fields with spatially variable mean, *J. Geophys. Res., 95*(8), 13543–13547, 1990.

Levitus, S., and T. P. Boyer (Eds.), *World Ocean Atlas 1994*, vol. 4, *Temperature*, Natl. Ocean. Data Cent., Silver Spring, Md., 1994.

Levitus, S., J. I. Antonov, and T. P. Boyer, Interannual variability of temperature at a depth of 125 meters in the North Atlantic ocean, *Science, 266*, 96–99, 1994a.

Levitus, S., R. Burgett, and T. Boyer (Eds.), *World Ocean Atlas 1994*, vol. 3, *Salinity*, Natl. Ocean. Data Cent., Silver Spring, Md., 1994b.

Maier-Reimer, E., U. Mikolajewicz, and A. Winguth, Future ocean uptake of CO₂: Interaction between ocean circulation and biology, *Clim. Dyn., 12*, 711–721, 1996.

Millero, F. J., Thermodynamics of the carbon dioxide system in the oceans, *Geochim. Cosmochim. Acta, 59*(4), 661–677, 1995.

Morel, A., Optical modeling of the upper ocean in relation to its biogenous matter content (case I waters), *J. Geophys. Res., 93*(9), 10749–10768, 1988.

Musgrave, D. L., Numerical studies of tritium and helium-3 in the thermocline, *J. Phys. Oceanogr., 20*, 344–373, 1990.

Neftel, A., H. Friedli, E. Moor, H. Lötscher, H. Oeschger, U. Siegenthaler, and B. Stauffer, Historical CO₂ record from the Siple station ice core, in *Trends '93: A Compendium of Data on Global Change*, edited by T. Boden et al., *Rep. ORNL/CDIAC-65*, pp. 11–14, Carbon Dioxide Inf. Anal. Cent., Oak Ridge Natl. Lab., Oak Ridge, Tenn., 1994.

Oceanographic Data Facility, South Atlantic Ventilation Experiment (SAVE), Legs 1-3, *Chem., Phys. and CTD Data Rep., 92-9*, Scripps Inst. of Oceanogr., La Jolla, Calif., 1992a.

Oceanographic Data Facility, South Atlantic Ventilation Experiment (SAVE), Legs 4-5, *Chem., Phys. and CTD Data Rep., 92-10*, Scripps Inst. of Oceanogr.,La Jolla, Calif., 1992b.

Parrilla, G., A. Lavin, H. Bryden, M. Garcial, and R. Millard, Rising temperatures in the subtropical North Atlantic ocean over the past 35 years, *Nature, 369*, 48–51, 1994.

Physical and Chemical Oceanographic Data Facility, Transient tracers in the ocean: North Atlantic Study, *Shipboard Phys. and Chem. Data Rep, 86-15*, Scripps Inst. of Oceanogr, La Jolla, Calif., 1986a.

Physical and Chemical Oceanographic Data Facility, Transient tracers in the ocean: Tropical Atlantic Study, *Shipboard Phys. and Chem. Data Rep.*, 86-16, Scripps Inst. of Oceanogr., La Jolla, Calif., 1986b.

Poisson, A., and C.-T. A. Chen, Why is there so little anthropogenic CO₂ in the Antarctic Bottom Water?, *Deep Sea Res., Part A, 34*(7), 1255–1275, 1987.

Quay, P. D., B. Tilbrook, and C. S. Wong, Oceanic uptake of fossil fuel CO₂: Carbon-13 evidence, *Science, 256*, 74–79, 1992.

Redfield, A. C., B. H. Ketchum, and F. A. Richards, The influence of organisms on the composition of sea-water, in *The Sea*, vol. 2, edited by M. N. Hill, pp. 26–77, Wiley-Interscience, New York, 1963.

Reid, J. L., W. D. Nowlin, and W. C. Patzert, On the characteristics and circulation of the southwestern Atlantic Ocean, *J. Phys. Oceanogr., 7*, 62–91, 1977.

Robitaille, D. Y., and A. J. Weaver, Validation of sub-grid-scale mixing schemes using CFCs in a global ocean model, *Geophys. Res. Lett., 22*(21), 2917–2920, 1995.

Roether, W., R. Schlitzer, A. Putzka, P. Beining, K. Bulsiewicz, G. Rohardt, and F. Delahoyde, A chlorofluoromethane and hydrographic section across Drake Passage: Deep water ventilation and meridional property transport, *J. Geophys. Res., 98*(8), 14423–14435, 1993.

Rooth, C., and H. Östlund, Penetration of tritium into

the Atlantic thermocline, *Deep Sea Res. Oceanogr. Abstr., 19*(7), 481–492, 1972.

Sabine, C. L., D. W. R. Wallace, and F. J. Millero, Survey of CO$_2$ in the oceans reveals clues about global carbon cycle, *Eos Trans. AGU, 78*(5), 49, 54–55, 1997.

Sarmiento, J. L., and C. LeQuéré, Oceanic carbon dioxide uptake in a model of century-scale global warming, *Science, 274*, 1346–1350, 1996.

Sarmiento, J. L., C. G. H. Rooth, and W. Roether, The North Atlantic tritium distribution in 1972, *J. Geophys. Res., 87*(10), 8047–8056, 1982.

Sarmiento, J. L., J. C. Orr, and U. Siegenthaler, A perturbation simulation of CO$_2$ uptake in an ocean general circulation model, *J. Geophys. Res., 97*(3), 3621–3645, 1992.

Sarmiento, J. L., C. LeQuéré, and S. W. Pacala, Limiting future atmospheric carbon dioxide, *Global Biogeochem. Cycles, 9*(1), 121–137, 1995a.

Sarmiento, J. L., R. Murnane, and C. LeQuéré, Air-sea CO$_2$ transfer and the carbon budget of the North Atlantic, *Philos. Trans. R. Soc. London, Ser. B, 348*, 211–219, 1995b.

Schlosser, P., B. Kromer, R. Weppernig, H. H. Loosli, R. Bayer, G. Bonani, and M. Suter, The distribution of ^{14}C and ^{39}Ar in the Weddell Sea, *J. Geophys. Res., 99*(5), 10275–10287, 1994.

Schlosser, P., G. Bönisch, B. Kromer, H. H. Loosli, B. Bühler, R. Bayer, G. Bonani, and K. P. Koltermann, Mid-1980s distribution of tritium, ^{3}He, ^{14}C and ^{39}Ar in the Greenland/Norwegian seas and the Nansen basin of the Arctic ocean, *Progr. Oceanogr., 35*, 1–28, 1995.

Shiller, A. M., Calculating the oceanic CO$_2$ increase: A need for caution, *J. Geophys. Res., 86*(11), 11083–11088, 1981.

Shiller, A. M., Reply to comment by Chen et al., on "Calculating the oceanic CO$_2$ increase: A need for caution" by A. M. Shiller, *J. Geophys. Res., 87*(3), 2086, 1982.

Siegenthaler, U., and F. Joos, Use of a simple model for studying oceanic tracer distributions and the global carbon cycle, *Tellus, Ser. B, 44*, 186–207, 1992.

Sievers, H. A., and W. D. Nowlin, The stratification and water masses at Drake Passage, *J. Geophys. Res., 89*(6), 10489–10514, 1984.

Smethie, W. M. J., Tracing the thermohaline circulation in the western North Atlantic using chlorofluorocarbons, *Progr. Oceanogr., 31*, 51–99, 1993.

Smethie, W., H. Ostlund, and H. Loosli, Ventilation of the deep Greenland and Norwegian Seas: Evidence from krypton-85, tritium, carbon-14 and argon-39, *Deep Sea Res., Part A, 33*, 675–703, 1986.

Smethie, W., D. Chipman, J. Swift, and K. Koltermann, Chlorofluromethanes in the Arctic Mediterranean Seas: Evidence for formation of bottom water in the Eurasian Basin and deep-water exchange through Fram Strait, *Deep Sea Res., Part A, 35*, 347–369, 1988.

Stocker, T. F., W. S. Broecker, and D. G. Wright, Carbon uptake experiments with a zonally averaged global ocean circulation model, *Tellus, Ser. B, 46*, 103–122, 1994.

Swift, J., A recent θ-S shift in the deep waters of the northern North Atlantic, in *Climate Processes and Climate Sensitivity, Geophys. Monogr. Ser.*, vol. 29, edited by J. Hansen and T. Takahashi, pp. 39–47, AGU, Washington, D. C., 1984.

Takahashi, T., and P. Brewer, Hydrographic and chemistry data for the TTO/NAS expedition, April - October, 1981: Revised carbon chemistry data, *lett. to CDIAC*, Carbon Dioxide Inf. Anal. Cent., Oak Ridge Natl. Lab., Oak Ridge, Tenn., 1986.

Takahashi, T., R. A. Feely, R. Weiss, R. H. Wanninkhof, D. W. Chipman, S. C. Sutherland, and T. T. Takahashi, Global air-sea flux of CO$_2$: An estimate based on measurements of sea-air pCO$_2$ difference, in *Revelle Symposium: Proceedings of the National Academy of Science*, edited by C. D. Keeling, vol. 94, pp. 8292–8299, Natl. Acad. Sci., Washington, D. C., 1997.

Tans, P. P., J. A. Berry, and R. F. Keeling, Oceanic ^{12}C/^{13}C observations: A new window on ocean CO$_2$ uptake, *Global Biogeochem. Cycles, 7*(2), 353–368, 1993.

Thiele, G., and J. L. Sarmiento, Tracer dating and ocean ventilation, *J. Geophys. Res., 95*(6), 9377–9391, 1990.

Toggweiler, J. R., K. Dixon, and K. Bryan, Simulations of radiocarbon in a coarse-resolution world ocean model, 1, Steady state prebomb distributions, *J. Geophys. Res., 94*(6), 8217–8242, 1989a.

Toggweiler, J. R., K. Dixon, and K. Bryan, Simulations of radiocarbon in a coarse-resolution world ocean model, 2, Distribution of bomb-produced carbon 14, *J. Geophys. Res., 94*(6), 8243–8264, 1989b.

Tsunogai, S., T. Ono, and S. Watanabe, Increase in total carbonate in the Western North Pacific water and a hypothesis on the missing sink of anthropogenic carbon, *J. Oceanogr., 49*, 305–315, 1993.

Uppström, L., The boron/chlorinity ratio of deep-sea water from the Pacific Ocean, *Deep Sea Res. Oceanogr. Abstr., 21*(1), 161–162, 1974.

Veronis, G., The role of models in tracer studies, in *Numerical Models of the Ocean Circulation*, pp. 133–146, Nat. Acad. of Sci., Washington, D. C., 1975.

Wallace, D. W. R., Monitoring global ocean carbon inventories, *OOSDP Background Rep. 5*, Ocean Obs. Syst. Dev. Panel, Texas A&M Univ., College Station, 1995.

Warner, M. J., and R. F. Weiss, Solubilities of chlorofluorocarbons 11 and 12 in water and seawater, *Deep Sea Res., Part A, 32*(12), 1485–1497, 1985.

Warner, M. J., and R. F. Weiss, Chlorofluoromethanes in the South Atlantic Antarctic Intermediate Waters, *Deep Sea Res., Part A, 39*(11/12), 2053–2075, 1992.

Weiss, R., Carbon dioxide in water and seawater: The solubility of non-ideal gas, *Mar. Chem., 2*, 203–215, 1974.

Weiss, R., J. Bullister, R. Gammon, and M. Warner, Atmospheric chlorofluoromethanes in the deep equatorial Atlantic, *Nature, 314*, 608–610, 1985.

Weiss, R. F., M. J. Warner, P. K. Salameh, F. A. VanWoy, and K. G. Harrison, South Atlantic Ventilation Experiment, *SIO Chlorofluorocarbon Meas., 93-49*, Scripps Inst. of Oceanogr., La Jolla, Calif., 1993.

N. Gruber, AOS Program, Princeton University, Princeton, NJ 08544. (e-mail: gruber@splash.princeton.edu)